

Contents lists available at ScienceDirect

Cleaner Energy Systems

journal homepage: www.elsevier.com/locate/cles



Freshwater Production Towards Microgrid Integration: Physics, Progress, and Prospects of Solar-Thermal Evaporation



Md Mahmudul Hasan*, Boker Agili, Ishtiaque Zaman, Miao He, Michael Giesselmann

Department of Electrical and Computer Engineering, Texas Tech University, Lubbock, Texas-79409, USA

ARTICLE INFO

Keywords: solar thermal evaporation carbon-based absorber interfacial heating power generation microgrid and desalination

ABSTRACT

Solar-thermal evaporation is an ancient system that generates thermal-induced vapor utilizing solar energy, which is renewable, clean, and has negligible environmental footprints. Though old, this system has recently revived tremendous attraction to the science community because of synthesized high-absorptive materials, smart heat and vapor management, and engineering marvels in device configurations. Integrated as a whole, the solar-thermal evaporation system facilitates improved solar to vapor conversion efficiency at low capital costs. In this review, a comprehensive discussion of physics, chemistry, and engineering behind solar-thermal evaporation systems has been presented in a summary manner. Moreover, this paper potentially addresses freshwater production techniques from sea or wastewater and nexuses some innovative approaches to generate electrical power. This review also presents emerging research activities in various aspects of solar-thermal evaporation with some interesting findings and points out critical advancement deficiencies. The futuristic view of microgrid system integration is also discussed extensively to nexus electrical power generation cleanly. This paper intends to present a comprehensive assessment of current advances in STE systems to encourage primary and practical research in leveraging underutilized supplemental energy sources for future integration of water, energy, and environmental systems with promised research direction and advancement.

1. Introduction

Critical considerations are required to reduce dependency on fossil fuels such as petroleum, coal, and natural gas due to their adverse environmental impacts and limited availability. Alternative renewable energy sources, for example, solar energy (Huang et al., 2016), wind energy (Okumus and Dinler, 2016), tidal energy (Uihlein and Magagna, 2016), and geothermal energy (Fridleifsson, 2001), become handy since their generation and utilization are clean, environmentally friendly, cost-effective, and sustainable.

Among them, solar energy is an abundant and promising energy source for next-generation commercial and domestic power applications. The received solar power by the earth's surface is approximately 1.08×10^{14} kW (Figure 1a). Only 0.1% of this energy can generate 3×10^{3} GW electrical power is four times greater than total electricity production worldwide (Thirugnanasambandam et al., 2010). Though not mass harnessing, to date, this solar energy has been extensively utilized in many domestic and commercial applications, for example, hydrogen production (Steinfeld, 2005), thermal power generation (Tina et al., 2006), PV-based electrical power generation (Lewis, 2016), photocataly-

sis (Chen et al., 2011), and solar-thermal evaporation (STE) (Banat et al., 2007).

In contrast with the renewable system, a massive volume of steam can be produced by burning fossil fuels in conventional technologies such as steam-based plants. It also by-produces hazardous residues, which is concerning for environmental and health issues (Goto et al., 2013). In another clean route, steam generation occurs at boiling point using concentrated solar irradiation (Blanco et al., 2009). In this process, the conventional working fluid, which has a better thermal capacity, is employed to heat the water and change the phase to steam. This route, generally named conventional solar-driven steam generation, uses a lot of optical devices to concentrate the solar irradiation focusing on the working fluid, which leads to high infrastructure costs but low thermal conversion efficiency (Blanco et al., 2009). The science communities have made many efforts to reduce costs and leverage their effectiveness. Conventional solar-driven systems include, but are not limited to, solar-based power plants, solar water heaters, solar chimneys, solar driers and cookers, solar-based evaporation, solar ponds, and stills (Figure 2) (Qiblawey and Banat, 2008).

E-mail addresses: md-mahmudul.hasan@ttu.edu (M.M. Hasan), boker.agili@ttu.edu (B. Agili), ishtiaque.zaman@ttu.edu (I. Zaman), miao.he@ttu.edu (M. He), michael.giesselmann@ttu.edu (M. Giesselmann).

^{*} Correspondence:

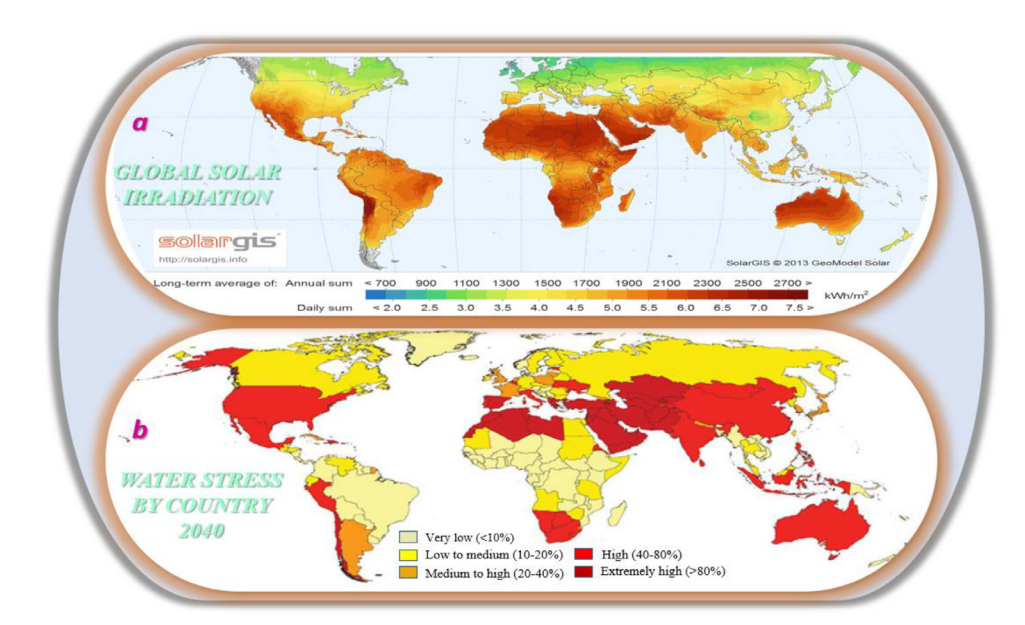


Figure 1. Solar irradiation and freshwater distribution by countries around the world. a. global horizontal solar irradiation projection, b. estimated water scarcity by countries in 2040

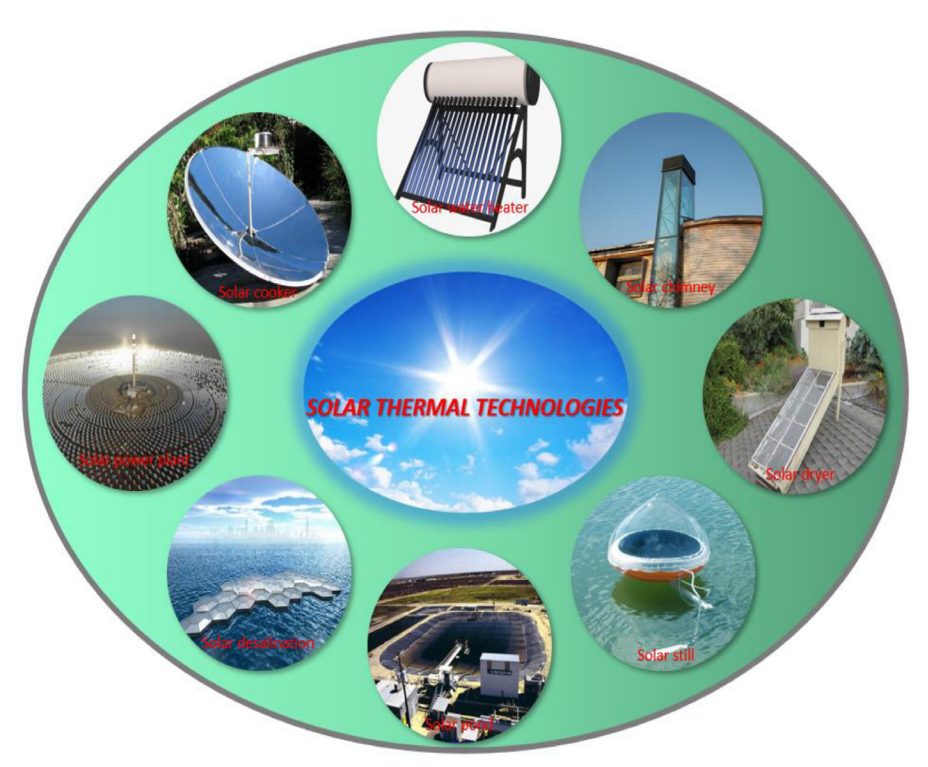


Figure 2. The existing solar-based energy harvesting systems, solar power plant, solar cooker, solar water heater, solar chimney, solar dryer, solar desalination, solar pond, and solar still.

STE-enabled vapor generation is one of the most promising and emerging solar-driven systems due to abundant natural resources, i.e., sunlight, seawater, and other water resources. Moreover, it is cost-free, environmentally friendly, and sustainable. In terms of potable water, scarcity of freshwater has been a significant concern for social welfare and people's health in recent years. Around 66% of the earth's population, approximately four billion, currently live under the scarcity line for at least one month a year (Mekonnen and Hoekstra, 2016). This picture will be much scarier by 2040 due to the ever-growing population, agricultural farms, and industries (Figure 1b) (Neto, 2018). It is necessary to enhance freshwater output from diverse sources, such as the ocean, river, lake, polluted reservoirs, etc., in order to satisfy expected demand. Using traditional methods to generate large quantities of freshwater entails costly capital expenditures and poor conversion efficiencies, which hinders expectations. Recent inventions of high absorptive photothermal materials and smart systems engineering revive solar-thermal

evaporation with high efficiency but low capital costs. Moreover, some innovative STE device engineering has incorporated electrical power generation along with freshwater generation (Li et al., 2022). Though this power generation is still in its early stages, it is foreseen that extensive research will enable STE-based power generation in commercialization.

Solar-thermal evaporation STE is a renewable energy process and recently has gained remarkable attraction owing to its diverse applications. In an STE system, a highly light absorptive material can absorb solar energy efficiently and convert it to heat to produce vapor from the surrounding water (Sattar et al., 2020). For STE-based freshwater production and power generation, high absorptive materials and specially engineered device structures are the first and foremost essential things. In recent years, novel and highly absorptive evaporators have attracted STE researchers due to their very high light absorptance, smart heat and mass management, long-term stability, and durability; hence, they are

very efficient. This novel converter avoids the need for costly optical concentrators with the help of very high light-capturing capabilities in the wide bandwidth of the sunlight spectrum from the visible-near infrared (NIR) region (Deng et al., 2017). Nowadays, gained with appreciation, the STE system can be utilized in harnessing electric power, medical instrument sterilization or sanitization, hydrogen fuel production, mechanical energy extraction, separation of liquids, waste water treatment, and mainly water purification and desalination, etc. (Kashyap and Ghasemi, 2020). However, large-scale commercialization of STE is still not achievable due to several existing issues such as lower efficiency, durability, stability, etc. (Pang et al., 2020). The researchers put a lot of effort into resolving these issues and enhancing conversion efficiency.

The main goal of STE-based research is to utilize abundant solar energy to co-generate power and freshwater. Many reviews have been carried out in the science communities to acknowledge this research in the last few years. If carefully observed, most of the review articles focus on various aspects of STE systems like absorber materials, physics, and chemistry of the STE system, device structure, desalination and purification, power generation, etc., individually. The state-of-the-art and novelty of their works primarily lie in specific aspects of STE systems. For example, some group presented their review focusing mainly on absorber materials, chemistry, and chemical engineering. Chen et al. mainly focused on evaporators' structural design and materials properties like light absorption, thermal management, water transport, etc. (Chen et al., 2019a). Fillet et al. extensively described various materials, mainly biological, and their derivatives as effective evaporator materials (Fillet et al., 2021). Pang et al. specifically presented the chemistry and materials engineering of STE devices. They used text mining and analytics algorithm to deliver the solar thermal evaporation review in a summary manner (Pang et al., 2020). Jin et al. systematically reviewed various types of nanomaterials for solar thermal evaporation (Jin et al., 2019). Zhao et al. reviewed materials design and engineering summary to present water-materials interactions (Zhao et al., 2020a). Dao et al. extensively discussed various types of carbon derivatives, like graphene, CNTs, graphite, carbon composite, black carbon, etc., for efficient solar-thermal conversion (Dao and Choi, 2018). Deng et al. presented an overall summary of recent findings of solar-driven evaporation with a plasmonic-based materials outlook (Deng et al., 2017). On the other hand, some groups focused on the evaporation mechanism and the ruling physics behind the STE system beyond materials science. Zhou et al. presented an extensive overview of the interfacial evaporation mechanism with a discussion on the rational design of the STE system (Zhou et al., 2019). Some other groups mainly focused on various applications of STE technology, such as vapor generation (Shi et al., 2020), evaporation-induced power generation and off-grid integration (Dao et al., 2021), simultaneous steam and power co-generation (Liu et al., 2020), hybrid interfacial systems with various applications like power, vapor, fuel, sterilization, etc. (Ding et al., 2021). However, a little attempt has been made to present a combined discussion of all aspects, for example, absorber materials, physics, and chemistry of the STE system, device structure, desalination and purification, power generation, etc., in a single review. To fill this gap, this review extensively discusses all aspects, such as physics, chemistry, and engineering of solar thermal evaporation, with recent findings. Moreover, this article elaborately presents the various exciting applications of STE systems, especially renewable electricity generation, along with the synergy concept. As a state-of-the-art novelty, this review also introduces the futuristic view of microgrid integration of the STE system in a power system manner. This study aims to give a complete review of current advancements in STE systems to promote primary and applied research in using underused supplementary energy sources for the future integration of water, energy, and environmental systems with the potential of research progress.

The purpose of this article is to provide a comprehensive summary of the most up-to-date developments in STE systems, as well as the essential advanced ideas that enhance the use of solar power. This ar-

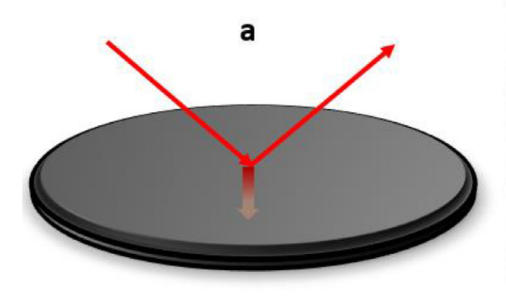
ticle starts with a detailed review of the state-of-the-art of STE, with the advancement in photothermal conversion and thermal management techniques. In the following section, a reader will find an elaborate discussion of the physics behind solar-thermal evaporation (STE), the mechanism and classification, and the ruling characteristics of the STE. Section three presents an observant review of carbon and its derivativebased devices, structure, and current findings. Section four highlights plasmonic-based STE with an elaborate but critical discussion. Hence, section five explores evaporators' smart and innovative structural design and engineering strategies to optimize STE performances. In the application section, along with electrical power generation, the futuristic view of microgrid integration is also discussed extensively. The current challenges and prospects are also presented at the end of this literature to provide a clear vision of the future STE system. This analysis seeks to educate readers about the many methods that might work together to maximize an STE system's potential for efficient solar energy use beyond just freshwater production.

2. Methodology for Selecting Literature Sources

The STE topic came to the table while considering cleaner energy generation for coastal area microgrid systems. It was seen that a hybrid solar-thermal evaporation system could produce enough fresh water along with thermal-based electricity. This study aims to create a map of the information accumulated by researchers working in the field of solar thermal evaporation (STE) technologies and the uses of STE technologies in a nexus of freshwater and energy production. As a consequence, the best practices are used in order to investigate the contributions made by the researchers in the published works. At first, we explored and studied the most recent review articles to find the gap to discuss. In order to determine keywords, the research area, and search tools, a technique for conducting a systematic review was developed. The procedure of review consisted of three primary stages: (i) the gathering of articles, (ii) the screening of the articles, and (iii) the evaluation of the articles that were chosen for further consideration.

In the beginning, the investigations are begun by taking into consideration the wide-area approach along with the kind of work that has been done by the researchers in the past. After that, we explored an extensive literature search using online tools such as Google Scholar, Researchgate, PubMed, etc. Solar-thermal evaporation, interfacial heating, plasmonic thermalization, heat localization, carbon-based blackbody absorption, evaporators' structure, electrical power generation, desalination, etc., were the main keywords in exploring peer-reviewed articles and journals. In the next step, the snowball approach is used in order to locate the papers that have been compiled from many peerreviewed journals in order to enhance the research. The search is carried out by utilizing websites and journals, for example, the Journal of Cleaner Production, Energy, Renewable Energy, Solar Energy, Renewable, Desalination, and Sustainable Energy Reviews. After that, the sources are enumerated, and a crystal-clear grasp of the knowledge gaps is produced. We collected more than five hundred articles on this topic and then sent them to the processing unit. During processing, we filtered out the necessary articles and assessed selected papers. The procedure of searching included papers from 1950 all the way up through 2022, with a primary focus on more recent publications. During the assessment, we faced some challenges, such as research credibility, online scams, misleading information, etc. Based on these challenges, we established three major criteria to assess the articles:

- Source reputation: We collected our articles from reliable peerreviewed journals.
- Validity: We cross-studied if the information/data provided in the article was valid or not.
- Credibility: We also evaluated the quality and credibility of the research work.



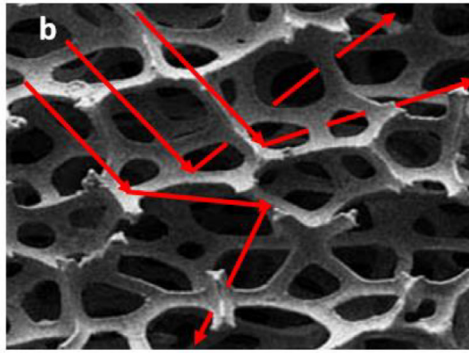


Figure 3. Untrapped and trapped light propagation. a. light reflection from a flat surface, and b. light trapping in the nano/micro-porous structure reduces the incident angle dependency. Schematic reproduced with the permission of ref. (Wang, 2018b).

After the assessment, we did an in-depth study to extract the most crucial information and data. We collected and scientifically tabulated data to present our review manuscript in a concise manner.

3. Solar-Thermal Evaporation Systems

Solar-thermal evaporation, STE, is a straightforward way to absorb sunlight using photo-thermal materials and convert it to thermal energy. Afterward, this thermal energy is collected by the nearby liquid (typically water) to generate vapor. In this system, loosely bound π -electrons of carbon-based materials and polaritons of plasmonic materials gain excitation energy by absorbing photons and rapidly releasing thermal energy via relaxation (Zhu et al., 2018a). During excitation, π -electrons of carbon-based materials gain enough energy to lift to the conduction band from the valance band (Richardson et al., 2009). On the other hand, in plasmonic materials, the Drude electrons of a metal couple with the incident photon at a particular resonant frequency or incident angle and subsequently create polaritons, which are the collective oscillations photon-electron pair (Yu et al., 2019). In both cases, the subsequent relaxation gives mechanical damping in the form of electron-electron, electron-phonon, and Rayleigh scattering (Zhang et al., 2016b). These mechanical damping induce phonons and thermalize the surroundings. Released thermal energy is then collected by water. The surrounding water gains enough energy to make a phase change, and hence, the vapor is generated. In general, when soaked by the photo-thermal materials, the photons induce an electromagnetic (EM) field that drives the charged carriers inside the materials and turns into heat while damping this kinetic energy of carriers (Liu et al., 2017b).

Vapor generation occurs at a lower temperature than the boiling point of water; on the other hand, steam generation occurs at or above the boiling point (Tao et al., 2018b). Though conventional photothermal materials capture photons efficiently, according to the Fresnel equation, they suffer high reflectance (>11%) due to their higher refractive index greater than 2. To minimize this reflective loss, a novel porous structure of the device becomes handy since it traps the light in the nano-porous cavity and eventually absorbs more than 96% of the light (Cai and Qi, 2015). Moreover, the porous structure reduces the incident angle dependency, enhancing the light absorptance, which is equally favorable to the solar-thermal conversion (Figure 3b) (Keshavarz Hedayati and Elbahri, 2016).

3.1. Classification of the Absorber

The STE can be classified into three categories based on the photothermal device location on liquid. First, **solar still**, where the photothermal receiver has placed at the bottom of the liquid (Figure 4a). In this system, solar to thermal conversion occurs at the surface of the receiver, but evaporation occurs elsewhere in the system (Kabeel and El-Agouz, 2011). This delocalized heat and vapor generation plus preheating of bulk water before absorption by the device leads to unavoidable heat and temperature drop, causing heat losses to a large extent

and driving the systems with poor performances (30-40% efficiency) (Kabeel and El-Agouz, 2011).

Second, **volumetric heating**, where the optical nanoparticles or nanofluids are homogenously dispersed all over the liquid and demonstrate moving heat generation through bulk water (Otanicar et al., 2010) hence, can achieve limited conversion efficiency (Figure 4b) (Ni et al., 2015). Though it reduces surface heat losses, it still suffers from bulk water heating. Moreover, compact dispersion and continuous pumping of nanoparticles to the interior of the liquid under long-term irradiation remain challenging (Yu et al., 2017).

The third is **interfacial heating**, where the photothermal device is placed at the interface of liquid and air (Figure 4c) (Gong et al., 2022). This approach ensures thermal confinement at the surface and suppresses bulk water heating, improving evaporation efficiency by around 90% under one sun illumination(Ghasemi et al., 2014). Also, interfacial heating has additional features, such as no volumetric loss, compact structure, and dynamic tunability of vapor flux and temperature, assuring diverse STE technologies in stand-alone, portable, and integrated systems (Ni et al., 2016b).

3.2. Evaporation Mechanism

In the previous contexts, it is evident that bottom and volumetric heating schemes suffer huge heat losses owing to bulk liquid thermalization. On the other hand, interfacial heating with heat localization has gained tremendous attraction in STE technologies, thanks to the evaporators' smart heat management concept. If the light is absorbed in the sub-molecular arena, the photon-to-phonon conversion is identical for every material, and it possesses almost 100% thermal conversion efficiency (Wang, 2018). To support this concept, the research on solar to the thermal conversion of MXene and carbon nanotubes (CNTs) reveals that the efficiency is almost close to 100% (Li et al., 2017a). Further studies of Ti_3O_4 and Au nanoparticles also support this finding (Wang et al., 2017b). Therefore, from the microscopic point of view, photon-particle interaction has no effect in the STE systems. To date, the hierarchy of STE technologies in volumetric and interfacial heating reveals that efficient vapor generation revolves around the following fundamental components. i. highly efficient absorber materials with light-trapping structures. ii. smart evaporator design enables two functionalities simultaneously, pumps the water to the active evaporation region, and aid vapor escape quickly. iii. innovative and compact thermal insulator design, which can effectively reduce bulk water heating.

The first critical step in choosing absorber materials is efficient light absorption over the broadband spectral range from UV to near-infrared (NIR) (Cao et al., 2015). This broadband spectral range ensures overall visible spectral absorption, which is mandatory and crucial for high-efficiency evaporation. Before excitation, the photon-particle interaction determines three fates of light; first, a portion of light can be reflected, based on the Fresnel equation, if the absorber's reflective index is higher than air. Conventional evaporators have a much higher reflective index (>2) and induce significant reflective losses (>11%). Reflective losses can be reduced by introducing light trapping configuration,

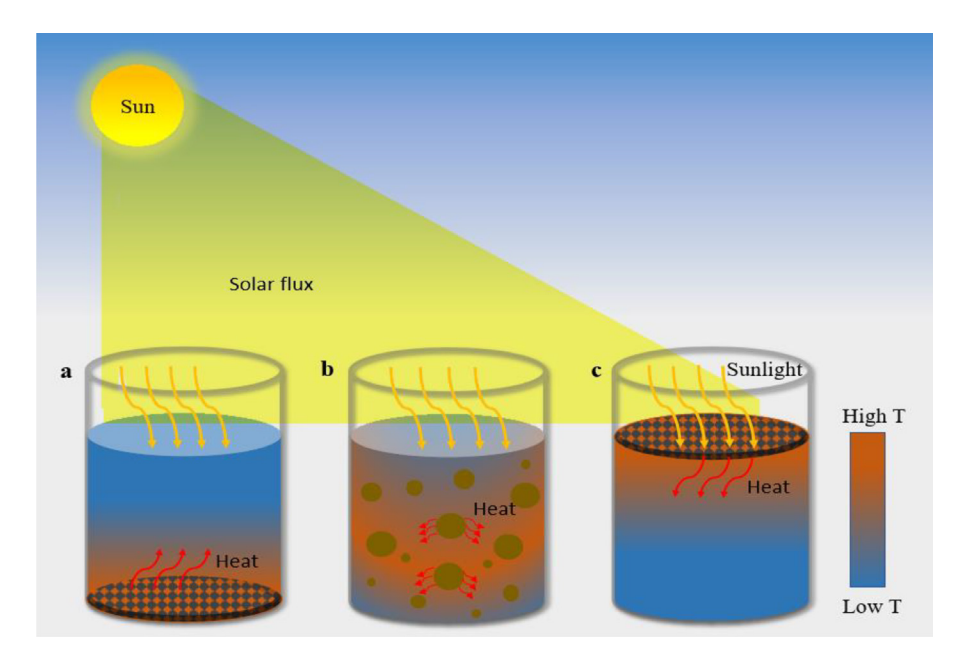


Figure 4. Schematic drawing of various types of STE-based water heating. a. solar still heating, b. volumetric heating, and c. interfacial heating.

cavity, and porosity. In the cavity or porous structure, the photons face multi-scattering, lose energy in every scattering, and eventually absorb the materials. Second, transmittance, a portion of light can be transmitted through the materials if the photon energy is less than the required energy to lift the electrons from the valance band to the conduction band in blackbody materials or couple with electrons and form polaritons in plasmonic materials. Conventional black carbon and its derivatives are semiconductor-type materials with almost zero bandgaps, with much lower light transmittance characteristics. Based on the Drude model, electron resides on the conduction band and can be coupled with the light efficiently to form polaritons in the plasmonic materials. Only some novel metals with negative permittivities, like gold, silver, and aluminum, show this optical phenomenon. Third, absorptance, if a photon's energy is equal to or greater than the energy required to transit electrons from the valance band to the conduction band, light absorption occurs in blackbody materials, and coupling with electrons in plasmonic materials at the resonant frequency (Xiong et al., 2015). For an efficient evaporator, it is critical to choose materials with very low reflectance and transmittance and almost perfect absorptance (>96%). Another way is to minimize reflectance and transmittance losses using an ideal absorber coating, enhancing the absorption over a broad spectral

After the relaxation, the excited particles lose the damping energy in the form of mid- or far-infrared radiation. This infrared radiation has a long wavelength and is blackbody type, which induces unnecessary thermal losses to the surroundings. Based on these discussions, though it can never be reached, an ideal absorber should have two contrasting characteristics: overall visible light absorption and near-zero infrared emittance. Suppressed thermal radiation losses can be achieved by employing spectrally selective coating. Which simultaneously has very high visible light absorptance and low infrared emittance. Applying spectrally selective coating assigns three main microscopic mechanisms: i. multilayer impedance matching based antireflection (García-Vidal et al., 1997), ii. involving high-density optical modes (Chou et al., 2014), and iii. nanostructures light coupling (Xi et al., 2007). The spectrally selective coating can mainly fabricate by the multilayer and metal-dielectric coating process on the metallic substrates (Ueno et al., 2018). Another way to induce selective coating is to coat blackbody materials and introduce surface texturing. A blackbody is a single material that can absorb a more comprehensive spectral range and is associated with a lowcost fabrication process (Zhang et al., 2017a). Surface texturing involves a modified porous structure, enhancing light trapping in the absorber (Peng and Qin, 2011).

The evaporator is placed homogeneously over the liquid in volumetric heating, forming active regions around the nanoparticles. In that case, pumping water to the active region coincides; hence, no unique design is required. But in interfacial heating, smart evaporator design with adequate liquid pumping from bulk water to the active region and proper vapor escaping are other crucial steps for efficient evaporation (Tao et al., 2018b). The wettability of the liquid transporting layers enables continuous pumping to the active zone. Conventional carbon and plasmonic materials are naturally hydrophobic, which means a meager water-wicking capability (Ito et al., 2015a). Adding ligands like -OH, $-NH_2$, -CO, -O- etc., commonly named functionalization, converts hydrophobic materials to hydrophilic (Ghasemi et al., 2014). Hydrophilic characteristics involve better water-wicking capabilities through the materials due to capillarity. This characteristic revolves around two main properties of materials (Ni et al., 2016a): i. microporous structure and ii. an adhesive force with a contact angle less than 90 degrees. Micro-porosity and the adhesive force between liquid and porous surface boost water wicking from the bottom to the top of the evaporator device. In this case, the smaller the diameter of pores indicates more significant the wicking. On the other hand, the more excellent the adhesiveness, the greater the wicking through the pores. Pores should be densely packed since it reduces thermal conductivity, restricting heat diffusion to the bulk liquid and the surroundings.

An ideal absorber should have two separate layers of proper water pumping and vapor escape. i. bottom layer is hydrophilic, porous, and has enough depth to block the heat transport to bulk water. ii. the top layer is hydrophobic, porous, and has less depth than the bottom layer. The top layer functionalities are water wicking above the localized heating zone to aid vapor escape as fast as possible. This layer is dry and hot enough to gain kinetic energy. The localized hot zone, where the solar-thermal conversion occurs, needs to be formed between these two layers for better performance. A hydrophobic layer is formed by reducing the ligand density on the top surface of anodic aluminum oxide (AAO)-supported Au NP films, and a separate wettability is investigated (Yu et al., 2015). It is observed that the thoroughly wetted bottom layer can pump water efficiently, and the top layer can vaporize water stably at higher rates. In contrast, the hot zone cannot be wet if the bottom layer is hydrophobic and less evaporation occurs. Meanwhile, many bubbles form around the bottom layer and restrict further water and heat transfer. Under intense irradiation (>1 sun), the formed bubbles multiply and eventually rupture the Au NP films.

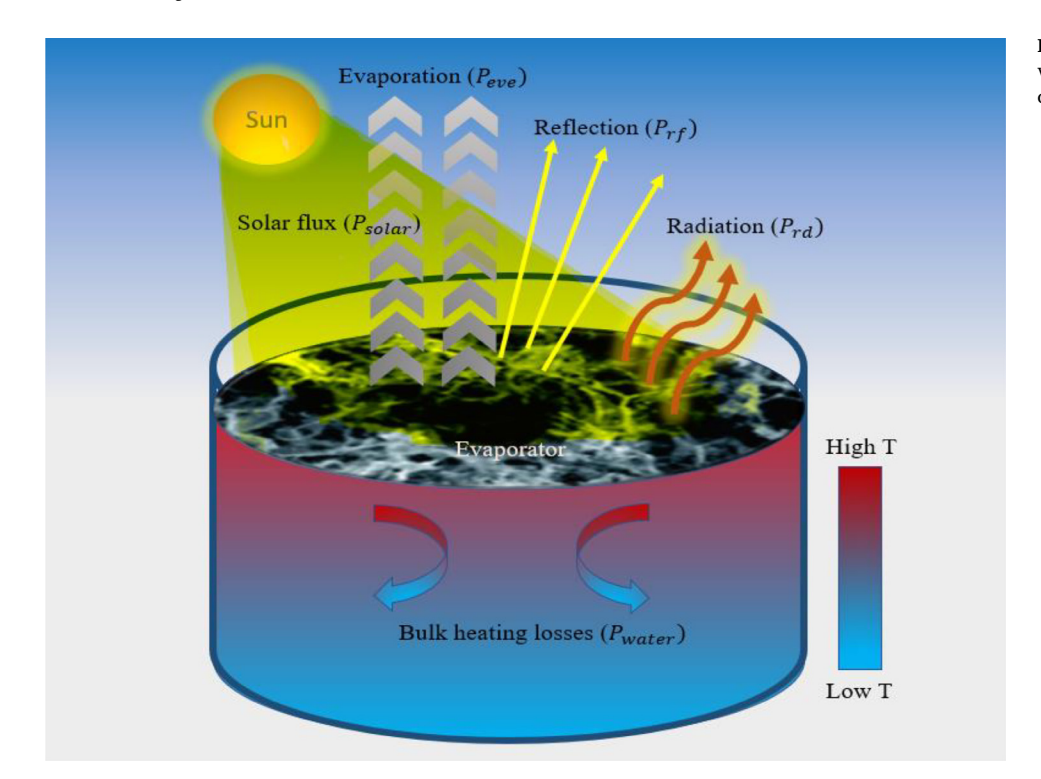


Figure 5. Associated losses and energy conservation schematic in standard solar-driven evaporation system

3.3. Associated Losses and Overall Performances

Continuous irradiation and solar-thermal conversion involve heat production and emission in various directions (Tiwari et al., 2003). The associated heat emission forms directional heat losses in the system and can be classified into five categories (Figure 5) (Wang, 2018): i. Top reflection heat loss (Prf), which is pre-solar-thermal conversion heat loss mainly causes due to the reflection of the sunlight from the surface. This can be minimized by employing selective antireflection coating at the top of the surface. ii. Top radiative loss (Prd), which associates heat loss after the conversion and radiates to the air in the form of mid- or far-infrared radiation. This radiative loss can be reduced by using selective photo coating, which permeates visible light but prevents longwavelength infrared radiation. iii. Top heat convection (Pcv, t) is air particles-carried heat loss in the upper medium. Proper vapor management at the top of the evaporator surface can minimize this type of loss by utilizing heat-sucking action by the vapor. iv. Bottom convection heat loss (Pcv, b), which is bulk water carried heat loss at the interior of the water and is the most effective form of heat loss. v. Bulk water conduction loss (Pcd, b), water's shallow heat conduction properties associate a small portion of heat loss in the water. Pcv, b and Pcd, b associate bulk water heating (Pwater) and significantly reduce overall solar-thermal conversion performance.

Solar-thermal conversion suffers greatly from P_{water} and it is crucial to minimize this for the sake of better performance. In that case, a proper thermal insulator between the evaporator and bulk water must be inserted to perform two functionalities simultaneously, reduce Pwater significantly and wick the water to the "hot zone" properly. A thermal insulation layer made of porous carbon foam contained air bubbles in the pores, significantly reducing Pwater since air has very low thermal conduction and excellent insulation properties. However, these densely closed pores contain capillary tubes needed to deliver water to the hot zone (Ghasemi et al., 2014). In another study, a thermal insulator (polystyrene foam) was placed between the liquid and the evaporator to suppress the downward heat loss (Li et al., 2016b). The polystyrene foam has no open pores, so no water is pumping through it. This insulator was wrapped up with hydrophilic cellulose to pump the water to the hot zone. Water was wicked up through this cellulose wrapping due to

its capillarity. In another recent study, the thermal insulator had drilled some holes to pump the upward water (Ni et al., 2016a). In this design, the surface contact between water and the hot zone was minimized significantly reducing downward heat losses.

The overall performance of the solar-thermal conversion system, η_{l-v} can be estimated in a steady-state condition. Initially, the conversion starts with increasing the performance of steeping. Eventually, it undergoes a steady-state condition, the maximized evaporation state of the equilibrium evaporation, commonly called equilibrium evaporation. Thermodynamically, in equilibrium evaporation, the evaporator first gains the thermal energy from the sunlight and then facilitates the vapor generation based on the ambient saturation point. The higher water temperature leads to a higher saturation pressure, which acquires more vapor in the ambient air, thus promoting evaporation. Better evaporator design drives evaporation faster, and poorly designed evaporator moves slowly to equilibrium. When the system is in an equilibrium state, the associated losses are the minimum, and hence, the STE efficiency η_{l-v} can be evaluated by the following equation 1(Pang et al., 2020),

$$\eta_{l-v} \; = \; \frac{P_{ev}}{C_{opt}.q} \; = \; \frac{\dot{m}h_{Lv}}{C_{opt}.q} \; = \; \frac{Q_t}{C_{opt}.q} \; \frac{\dot{m}h_{Lv}}{Q_t} \; = \; \eta_{l-t}\eta_{t-v} \eqno(1)$$

where, $\dot{m}=(m_{light}-m_{dark})/A$ is the phase-changed-liquid mass per unit area (A) of absorber under solar irradiation. h_{Lv} is the total evaporation enthalpy. h_{Lv} constitute two parts: i. phase-change enthalpy, Δh (2.57 MJkg $^{-1}$ at 1 atm of water). ii. temperature gradient enthalpy, Δh , where C (4.18 KJkg $^{-1}K^{-1}$) is the water-specific heat, and ΔT is the temperature change to vaporizing point from room condition. C_{opt} is the total optical density, and q is the one sun illumination intensity (1kW m^{-2}). Q_t is the gained thermal energy by the absorber, and η_{l-t} and η_{l-v} are the light-to-thermal and thermal-to-vapor conversion efficiencies, respectively. P_{ev} can be estimated by

$$P_{ev} = C_{opt}.q - P_{losses}$$
 (2)

where, $P_{losses} = P_{rf} + P_{rd} + P_{cv,t} + P_{water}$. P_{rd} is the radiative type loss and can be calculated by $P_{rad} = \mathcal{E}\sigma(T_2^4 - T_1^4)$, on the other hand, P_{water} is conduction type loss and can be calculated by $P_{con} = h(T_2 - T_1)$. Where $\mathcal{E} = emissivity$ of the absorber, $\sigma = Stephan-Boltzmann$ constant, h = coefficient of heat transfer, $T_2 = temperature$ of absorber and $T_1 = temperature$

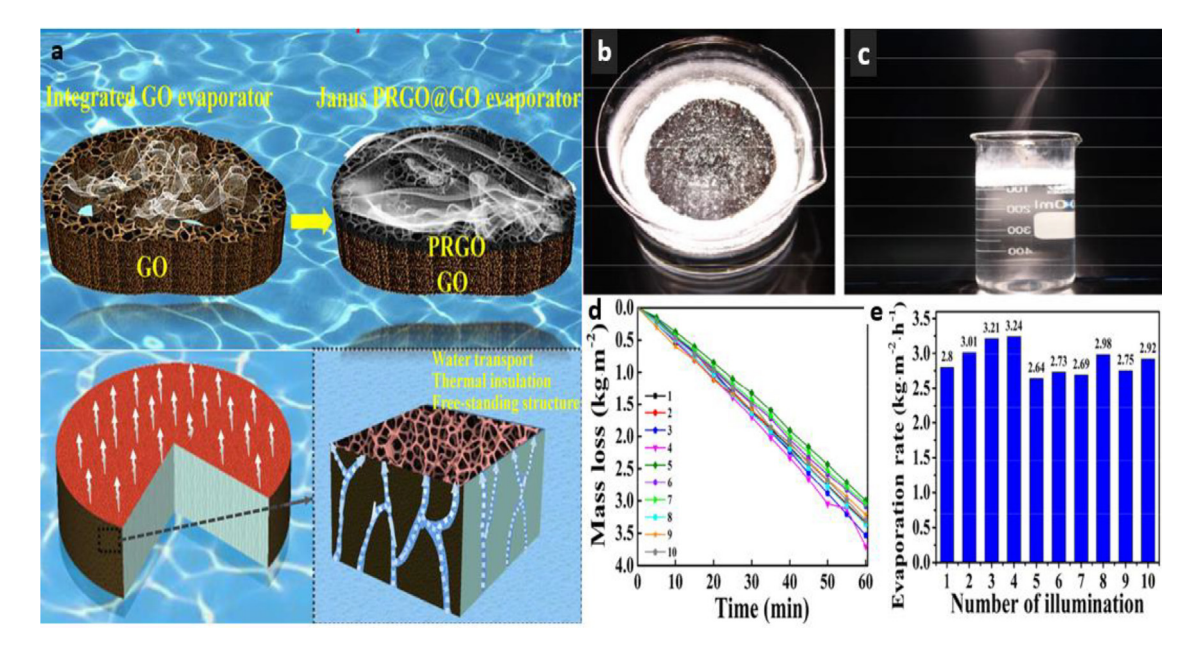


Figure 6. One illustration of the carbon-based photothermal absorber and STE conversion. a. Janus type GO hydrogel evaporator and formation process of PRGO@GO hydrogel during evaporation. b. self-floating GO hydrogel. c. vapor generation using PRGO@GO hydrogel. d. mass change reading under various solar illumination. e. various STE efficiencies of PRGO@GO hydrogel-based STE system under various solar illumination. Images reproduced with the permission of ref. (Chen et al., 2022).

temperature of the surroundings. P_{rf} and $P_{cv,t}$ are the reflective loss in air and convective loss in water, respectively. From equations 1 and 2,

$$\eta_{l-v} = 1 - \frac{P_{losses}}{C_{opt}.q}$$
 (3)

Based on equation 3, it is crystal clear that the overall performance only depends on associated losses P_{losses} . So, minimizing P_{losses} is the leading critical engineering to enhance overall performance.

4. Chemistry and Performances of STE Absorbers

The most critical part of the STE system for solar thermal evaporation is the evaporator. This evaporator absorbs the photon and converts it to heat. This evaporator must be highly light absorptive and low thermally conductive for efficient STE performances. Natural carbon and its derivatives, semiconductor materials, plasmonic materials, polymers, composite materials, etc., facilitate these features and are primarily used in the STE system (Figure 7).

4.1. Carbon and Its Derivatives

Carbon is naturally black and possesses blackbody absorption and emission while irradiated by solar energy. Some carbon derivatives exhibit sp^3 hybridization and form strong σ - σ bonds like C-C, C-H, and C-O, in which optical excitation over the energy gap is tiresome and needs enormous photonic energy. But, most of the carbon derivatives like carbon nanotube (CNTs) (Wang et al., 2016), graphene (Ito et al., 2015b), graphene oxide (GO) (Liu et al., 2017d), reduced graphene oxide (rGO) (Wang et al., 2018b), carbon black (Liu et al., 2015), carbon fabric and beads (Higgins et al., 2018), carbon air-laid foams (Chen et al., 2018), sponges (Zhu et al., 2018b) and carbonized other materials (Jia et al., 2017) consist sp^2 and sp hybridization and form weak π - π bonds, in which it is comparatively easy to optically excite the electrons to higher energy state from lower energy state. While relaxation, electrons undergo photon-phonon scattering and transfer mechanical vibration to the associated molecules (Vélez-Cordero and Hernández-Cordero, 2015). This phononic vibration of lattice generates infrared emissions and hence thermalizes quickly to the surroundings.

Carbon derivatives like graphene, carbon nanotubes (CNTs), charcoal, carbon black, etc., possess a broad spectrum of light absorption, high stability and durability, lightweight, and low fabrication cost. Unlike metallic absorbers, it is not degradable under intense solar irradiation and contains no toxicity. Hence they can be employed in water desalination and purification to a greater extent (Gao et al., 2019).

4.1.1. Pure and Reduced Graphene

To date, graphene-based absorbers have been extensively explored and utilized in the STE system due to their near-perfect light absorption, wide surface area, low molecular specific heat, high Debeye temperature, and chemically doping-based conductivity tunability (Ito et al., 2015a). Graphene can be employed as either nanofluid in the volumetric or floating evaporator in interfacial systems. It is also reported that graphene can act as a thermal insulator after proper functionalization. Utilizing in the volumetric system as a nanofluid, graphene must require hydrophilic properties. After oxidizing in the chemical vapor deposition (CVD) system, graphene gains enough hydrophilic property to smash and disperse in the liquid to act as a volumetric absorber. Rahman et al. reported that dispersed hydrophilic graphene shows 69% efficiency under ten sun irradiations (Rahman et al., 2017). 3D porous N-doped graphene was prepared by Ito et al. via CVD at different temperatures with micro-porosity and found 80% photothermal performance. The vapor generation rate was 1.50 kg $m^{-1}h^{-1}$ for nitrogen-doped graphene, which was annealed at a temperature of 950° C with an average pore size of 1-2 μ m under one sun illumination (Ito et al., 2017). The study also suggests that micrometer pore size shows better water-wicking capability than nano-sized pores. This phenomenon may occur with the sluggish water delivery in the nanoporous structures due to the viscosity suppression in the narrow pipe route. Some specially engineered graphene structure takes advantage of bandwidth tunability, for example, 3D structured graphene metamaterial (SGM) (Lin et al., 2020). SGM uses metallic trench-like features for wavelength selectivity and ultrathin graphene metamaterial layer for broadband dispersionless and good thermal conductivity. SGM absorbers provide great solar selective and omnidirectional absorption, wavelength tunability, good photothermal performance, and high thermal stability.

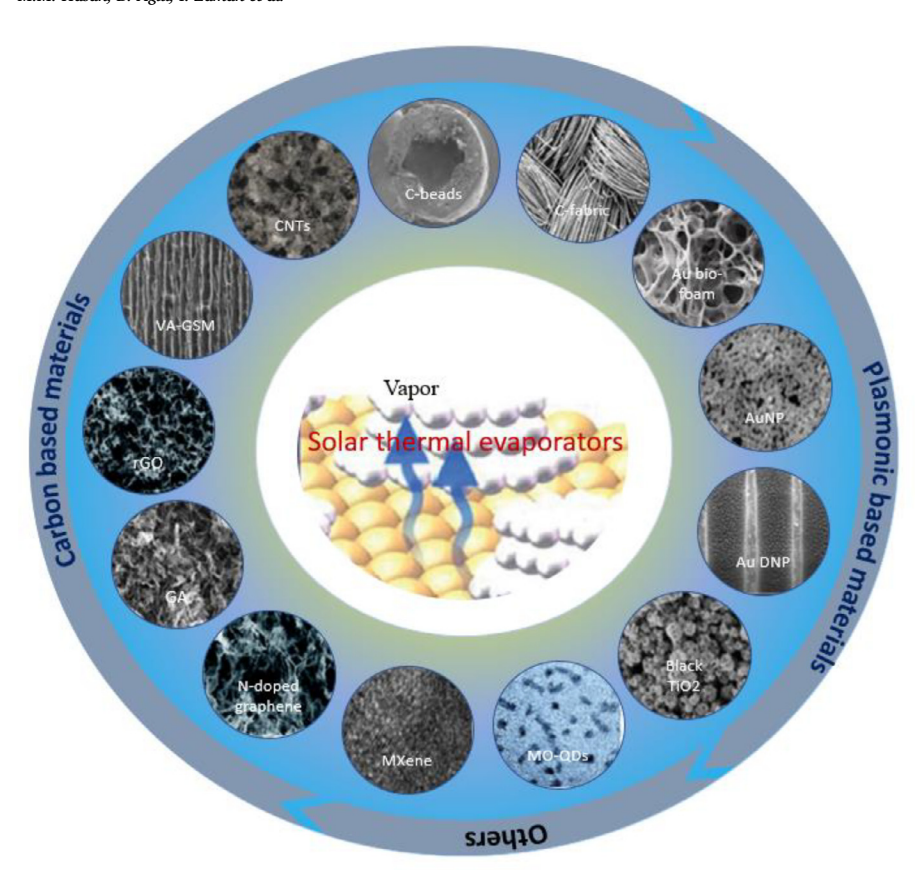


Figure 7. Representative presentation of some notable photothermal absorbers for efficient solar-thermal evaporation.

The graphene-based absorbers must have hydrophilic and low-density properties in the self-floating system. Fu *et al.* fabricated graphene aerogel (GA) using GO, enabling self-floating characteristics and rapidly pumping water to the hot zone. This configuration found conversion efficiencies of 53.6±2.5% and 82.7±2.5% at one and ten sun irradiations, respectively (Fu et al., 2017).

An innovative device was proposed by Chen et al., which can support essential characteristics of the STE system like high light absorption, porous, hydrophilic, better wicking capability, etc. A Janus-type graphene oxide (GO) hydrogel evaporator was manufactured to support their proposal and performed an STE experiment (Chen et al., 2022). At first, they synthesized integrated reduced GO hydrogels by chemically crosslinking process. The Janus type partially reduced graphene oxide PRGO nanosheet is automatically evolved on the top of the GO hydrogel during solar thermal evaporation (Figure 6a). This Janus type PRGO@GO hydrogel has high light absorptance (92.7%) and is naturally porous and highly hydrophilic, making this device a prominent candidate for the STE system. Furthermore, its floating and free-standing structure reduces losses to the surrounding. During the solar thermal experiment, this device shows a very high evaporation rate of 3.24 $kgm^{-2}h^{-1}$ with 99.98% conversion efficiency (Figure 6b,c,d&e).

Graphene can also be employed as a thermal insulator under the absorber and efficiently prevent downward thermal losses. In that case, the graphene needs to be hydrophilic, lightweight, and have enough micropores to deliver water to the active zone. Bian *et al.* manufactured the functionalized-graphene and observed improved photothermal efficiency of 38% to 48% under one sun illumination. Due to the capillarity, the functionalized-graphene is naturally hydrophilic and can enhance the continuous water pumping to the active zone (Bian et al., 2018). Some other notable graphene-based STE evaporators include, but not limited to, the graphene oxide layer on the porous wood (Liu et al., 2017d), vertically aligned-graphene sheets membrane (VA-GSM) (Zhang et al., 2017b), graphene oxide foam

(Li et al., 2021), polyvinylidene fluoride/graphene (Huang et al., 2021), rGO aerogel (Jian et al., 2021), graphene tube (Yin et al., 2021), etc.

4.1.2. Carbon Nanotube (CNTs) and Their Derivatives

Carbon nanotube (CNTs) is another potential candidate in carbon-based photothermal systems. Like graphene, CNTs are also employed in photothermal systems through nanofluids or suspension forms. Though potential candidates but its hydrophobic nature prevents direct implementation. One way to use CNTs in photothermal systems is to be treated with a base media (Hordy et al., 2014) or need to be plasma-based functionalization (Hordy et al., 2013). In a recent report, Chen et al. fabricated a CNT-modified flexible wood membrane to enhance STE efficiency, reduce fabrication costs, and broaden scale-up (Chen et al., 2017a). Since the wood membrane has excellent light absorption properties and low thermal conductivity, it showed improved efficiency of 81% under ten sun irradiations.

4.1.3. Other Carbon Materials

The resources of carbon-based materials are abundant in nature, and following their excellent photothermal properties, carbon-based materials are omnipresent and have gained tremendous attraction to the scientific communities (Rahman et al., 2017). Therefore, carbon materials are widely used in low-cost photothermal applications (Xue et al., 2017b). The primary conventional way to prepare carbon-based materials is to carbonize natural resources such as wood, bio-foams, beads, mushrooms, etc.

In a recent study, Xue *et al.* flame-treated a natural wood as a scalable, low-cost, and robust raw material for STE applications. The flame-treated wood absorber possesses near-perfect solar absorptance (99%), low thermal conductivity (0.33 Wm⁻¹K⁻¹) and enhanced hydrophilicity (Xue et al., 2017b). They also reported that this specially treated wood structure could localize the heat at the absorber surface and show 72% STE efficiency under one sun illumination. Xu *et al.* utilized mushrooms

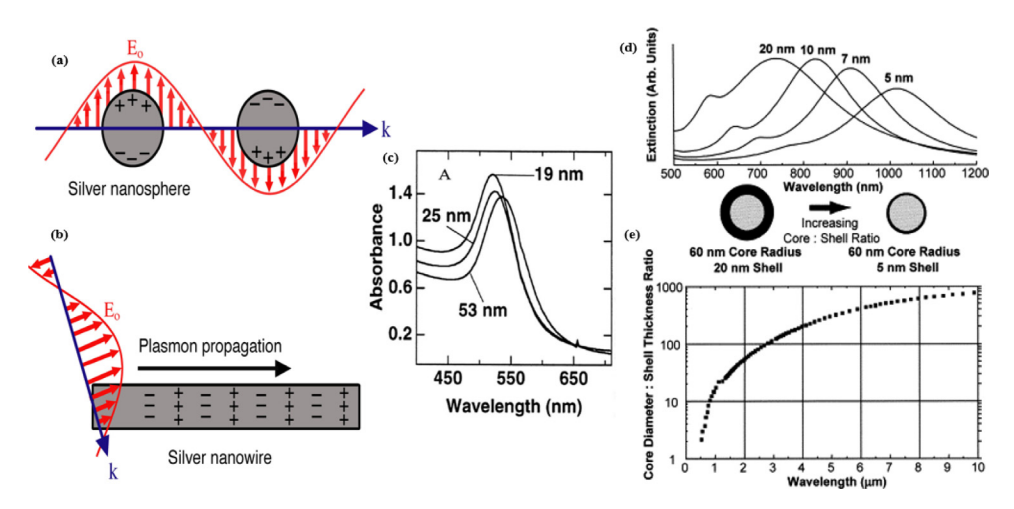


Figure 8. Illustration of plasmonic propagation, absorption, and extinction at a different wavelength, and size and shape dependency of plasmonic resonances. a. schematic of localized surface plasmons (LSPRs) model. b. schematic of surface plasmon polaritons (SPPs). Images reproduced with the permission of ref. (Rycenga et al., 2011). c. size and shape effect of 19 nm, 25 nm, and 53 nm gold nanoparticles. d. theoretical calculations of the extinction coefficient of metallic core-shell structures of silica/gold with various nano-sized particles. e. measurement of core radius/shell thickness ratio with resonance wavelength of core-shell structures. Images reproduced with the permission of ref. (Oldenburg et al., 1998).

as an efficient absorber after proper carbonization. Mushrooms have a unique structure, like, an umbrella-shaped black pileus, a porous stem, and a fibrous stipe with a small cross-section, enabling a better STE conversion (Xu et al., 2017b). Pre-and post- carbonizations of mushrooms show 62% and 78% STE efficiencies under one sun illumination, respectively. They also found that the distinctive features of the mushroom structure enable high light absorption, proper water pumping, and vapor escape and reduce bulk heat losses efficiently.

4.2. Plasmonic Materials

Surface plasmons are the collective oscillations of electromagnetic (EM) waves and Drude electrons at the metal-dielectric interface (Homola, 2003). The plasma approach of Maxwell's equations leads to the concept that the freely moving electrons at the metal's surface can couple with incident photons and originate non-radiative oscillations. These resonant phenomena are coherent and occur when the frequencies of photons and electrons perfectly match (Seh et al., 2012). Proper analysis of surface plasmon resonance reveals that only transversely magnetic (TM) polarized light can excite the electrons of metal, which has a higher refractive index than surroundings (normally dielectric) (Tang et al., 2010). The propagation constant of surface plasmon resonance β_{SP} can be expressed as(Maier et al., 2003),

$$\beta_{SP} = \frac{2\pi}{\lambda} \sqrt{\frac{\epsilon_{d} \epsilon_{m}}{\epsilon_{d} + \epsilon_{m}}} \tag{4}$$

where, $\varepsilon_{\scriptscriptstyle d}$ is the real part of dielectric permittivity, $\varepsilon_{\scriptscriptstyle m}$ is the real part of the metal's permittivity, and λ is the coupled wave's wavelength. Since the oscillation is non-radiative, the metal-dielectric waveguide supports only guided modes. Equation 4 suggests that the β_{SP} must need to be imaginary for guided mode propagation. As the permittivity of dielectric is normally positive, the permittivity of metal must be negative. Only some novel metals, such as gold (Au), silver (Ag), and aluminum (Al), possess a negative real part of permittivity in the visible and near-infrared light spectrum. The imaginary β_{SP} exhibits attenuation, b=0.2*Im (β_{SP})/ln (10) in terms of electron-electron scattering and eventually dissipate as heat. Two categories of the plasmonic phenomenon are cataloged so far (Xia and Halas, 2011); i. planar surface plasmon polaritons (SPPs), where the collective oscillations can travel across the xy plane of metal-dielectric interface for 10-100 μm with a penetration depth of about 100-600 nm in the wavelength region from 600-1000 nm. ii. localized surface plasmons (LSPs), in which metal nanoparticles (10-100 nm) are fixed and surrounded by free-electron clouds (Figure 8a&b).

In both models, three phenomena, near-field enhancement, hot electrons generation, and photothermal effect, occur sequentially. In the photothermal scheme, the plasmonic effect first generates "hot electrons" in terms of collective oscillation and eventually undergoes relaxation after releasing "phonons" (Webb and Bardhan, 2014). Hence

these phonons thermalize the surroundings like dielectric and metal (Brongersma et al., 2015). In this process, the heat transfer can occur within 100 picoseconds, and temperature ramps up to several thousand kelvins around the nanoparticles (El-Sayed, 2001).

The plasmon-induced photothermal effect depends on various factors, such as dielectric properties of metal and surroundings, size, shape, and 3D arrangement of the nanoparticles (Liz-Marzán, 2006). If the system is surrounded by air, the different composition of metals exhibits distinct absorption peaks. In the case of nanoparticles structure, it is investigated that other structures could lead to different maximum absorption wavelengths, λ_{max} . Oldenburg *et al.* designed a core-shell structure with SiO_2 as a core and Au as a shell. They intentionally varied the core and shell thickness to manipulate the λ_{max} . They found that variable thickness of core and shell can cover the whole visible to NIR spectra absorption (Oldenburg et al., 1998). So, it is evident that manipulating the surroundings and the size, shapes, and structure of nanoparticles allows the absorption wavelength to be tuned over visible to NIR spectra (Figure 8c, d&e).

As an illustration of a plasmonic-based STE system, metal-silicon (Si) hybrid nanowire (NWs) could be a great example of broad absorption range, low thermal losses, and enhanced conversion efficiency. To study the plasmonic-based STE system, Soo Joo et al. fabricated plasmonic-Si NWs bundles on a silicon wafer (Figure 9a) (Soo Joo et al., 2022). Silicon is naturally an excellent light absorber but cannot absorb higher wavelength photons due to its bandgap limitation. They deposited a metal (Au, Ni, Ti) layer around the Si nanowires (Figure 9b). These metal layers exhibit plasmonic characteristics like localized surface plasmon resonance for higher wavelength photons. So, metal-coated Si NWs can absorb a broad spectral range (300-2000 nm) with 91% absorptance. A microporous cellulose fiber (MCF) is used based on the absorber. This MCF ensures a better water-wicking capability to the absorber and suppresses bulk water heating. The low thermal conductivity of Si also enables heat localization at the absorber surface, reducing heat loss to the surroundings. After the fabrication and characterization of the plasmonic-Si NWs, they performed the STE experiment under one to ten sun illumination (Figure 9c&d). They found the overall evaporation rate is 1.12 $kgm^{-2}h^{-1}$ with 72.8% conversion efficiency under one sun irradiation.

Some other notable plasmonic materials such as 3D mesoporous wood with Au, Ag, and Pd nanoparticles (Zhu et al., 2018e), Al nanoparticles (Zhou et al., 2016b), germanium (Ge) nanocrystals (Sun et al., 2017), Ag-Au blended composites (Chen et al., 2016), Ag/Au bimetallic hollow mesoporous nanoshells (Zielinski et al., 2016), Au nanoparticles of AAO templates (Zhou et al., 2016a), Au metasurface (Liu et al., 2017a), metal nitrides (TiN, ZrN, HfN) (Margeson and Dasog, 2020), Ag/CuO-rGO nanocomposites (Kospa et al., 2021), Au dimer nanofluids (Chen et al., 2020) etc. have shown better heat localization and potential STE conversion efficiencies.

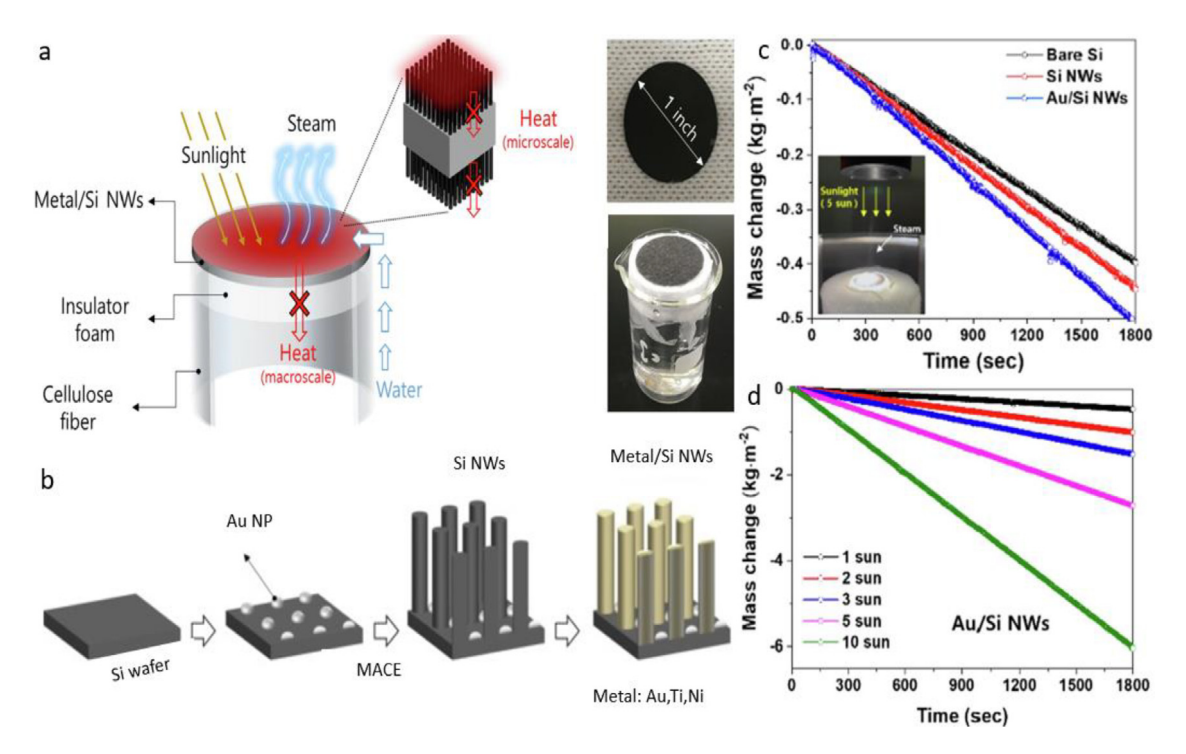


Figure 9. Illustrations of the plasmonic-based absorber and its use in the photothermal evaporation system. a. schematic of metal-Si NWs based solar thermal evaporation system with an actual photograph of the absorber and experimental device. b. metal-Si NWS bundle fabrication procedure. c. evaporation results over time for three types of the evaporator. d. evaporation results from various solar exposure. Images reproduced with the permission of ref. (Soo Joo et al., 2022)

4.3. Other Materials

Along with carbon and plasmonic-based materials, other materials like metal oxides, inorganic nanomaterials, and polymers show effective photothermal conversion due to their semiconductor-type behaviors (Table 1). In a semiconductor, the electrons on the valance band can absorb light and elevate to the conduction band if and only if the photon energy E_{ph} is equal or greater than the bandgap energy E_{g} of the materials. During relaxation, the electrons step down to the band edges of the conduction band from the elevation stage after releasing phonons. Hence, these phonons generate heat for the surroundings, and if the water is placed in the surrounding, it will heat up and produce vapor. The elevation of electrons to the conduction band also creates electronhole pairs in narrow bandgap materials and eventually recombines after the excitation, generating heat in terms of IR radiation (Umlauff et al., 1998).

To date, some other notable photothermal materials include, but not limited to, black titania (Zhu et al., 2016), spin-coated black ${\rm TiO_x}$ onto stainless steel mesh (Ye et al., 2017), magnetic nanofluids of ${\rm Fe_3O_4}$ (Shan et al., 2021), MnFe₂O₄, ZnFe₂O₄, and CuFe₂O₄ (Chen et al., 2017c), CuCr₂O₄/SiO₂ (Shi et al., 2018b), PbS nanoparticles (Jiang et al., 2013), Cu₃BiS₃ nanoflower on.

MXene (${\rm Ti_3C_2}$) (Wang et al., 2021), titanium nitride (TiN) (Ishii et al., 2016), hierarchical graphadiyne (Gao et al., 2017), ${\rm Cu_7S_4}$ (Zhang et al., 2016a), electrospun cadmium selenide nanoparticles-loaded cellulose acetate (Angel et al., 2020), nickel-embedded porous alumina (Wang et al., 2020), janus polypyrrole nanobelt (Zhao et al., 2021), and copper phosphate/PDMS (Hua et al., 2017). These materials also showed some significant photothermal performances in the lab experiments. Some specific polymers and their derivatives also exhibit photothermal performances. Polymers have better flexibility and moldability in water compared with inorganic materials. As-deposited polypyrrole (PPy) onto a porous steel mesh showed local heat enhancement and efficient photothermal conversion (Huang et al., 2017). In addition, polypyrrole-coated natural latex (PPy-NL) foam offers microporous wettability, high mechanical strength, and very high STE conversion ef-

ficiency of around 95% (Xu et al., 2020). Bacterial nano-cellulose (BNC) comprised of polydopamine (PDA), which is bio-degradable and environmentally friendly, showed better photothermal efficiency to about 78% under one sun illumination (Jiang et al., 2017, Wu et al., 2017b).

The previous discussion shows that carbon and its derivatives have high photothermal performance potential among various absorber material types. This phenomenon happens due to their abundance, ultrahigh light absorptance, cheap, low cost, easy fabrication, relative stability in water, and non-toxic. Though some other materials, such as plasmonic and polymer-based absorbers, exhibit reliable performances, some negative issues hinder large-scale applications. Plasmonic-based materials such as gold, silver, and aluminum are expensive; complex structures and fabrications are needed to cover the whole light spectrum and support a lot of parasitic losses in volumetric systems. On the other hand, semiconductor and polymer-based absorbers face some real challenges like relatively low absorptance, complex fabrication processes, and degradation nature in water for long-term usage.

5. STE System Device Architecture

Another crucial part of solar thermal evaporation is smart and innovative device architecture, along with absorber materials choice. A specially engineered device structure ensures better water and vapor transport, suppressed thermal losses, and light trapping capabilities. These features are critical in terms of efficient STE performances. So far, various pathway structures like 0D, 1D, 2D, 3D, and some bio-inspired designs have been investigated for solar thermal conversion.

5.1. 0D, 1D, 2D, and 3D Pathway Structure

For uninterrupted water transportation to the "hot zone" and efficient vapor generation, smart pathway design is the crucial factor facilitating reduced heat losses. So far, 0D, 1D, 2D, and 3D device structures have been utilized for smart water transportation.

Table 1
Some notable evaporator materials, device design concepts, and efficiencies.

Materials	Efficiency (%)	Solar intensity	Design of the device ^a	Reference		
Carbon sponge	90	1	Opten./Inwp.	(Zhu et al., 2018c)		
Black cellulose fabric	57±2.5	1	Ecw.	(Ni et al., 2018)		
Vertically aligned graphene sheets	86.5/94.2	1/4	Alst. /Ecw.	(Zhang et al., 2017b)		
Graphene foam	91.4	1-5	Opten.	(Ren et al., 2017)		
3D printed graphene oxide (GO)	85.6	1	Ecw.	(Li et al., 2017d)		
rGO-MWCNT membrane	80	1	Opten.	(Wang et al., 2018b)		
Carbon black-coated paper	88	1	Ecw.	(Liu et al., 2017e)		
Carbon black/GO	87.5	1	Ecw.	(Li et al., 2017c)		
rGO/filter paper	89.2	1	Ecw.	(Guo et al., 2017)		
GO film/cotton rod	85	1	Ecw.	(Shi et al., 2018a)		
Porous rGO layer	83	1	Ecw.	(Shi et al., 2017)		
GO film/cellulose paper	80	1	Ecw.	(Li et al., 2016a)		
Defect abundant graphene sheets	91	1	Ecw.	(Zhang et al., 2018b)		
rGO/polyurethane foam	81	10	Opten.	(Wang et al., 2017a)		
Vertically graphene pillar array	95	1	Alst.	(Zhang et al., 2018a)		
3D graphene networks/wood	91.8	1	Opten./Inwp.	(Kim et al., 2018)		
3D honeycomb graphene foam	87	1	Opten.	(Yang et al., 2018)		
Hierarchical graphdiyne based architecture	91	1	Opten.	(Gao et al., 2017)		
Carbon black in PVA	53.8	0.7	Pmd/Opten.	(Dongare et al., 2017)		
Black carbonized wood	91.3	1	Opten./Alst./Ecw.	(Liu et al., 2018b)		
Graphite/wood	80/89	1/10	Alst.	(Li et al., 2018b)		
CNT modified flexible wood	81	10	Alst.	(Chen et al., 2017b)		
Surface carbonized longitudinal wood	89	10	Alst.	(He et al., 2019)		
Carbonized wood	86.7	10	Opten./Alst.	(Jia et al., 2017)		
Flame treated wood	72/81	1/3	Alst.	(Xue et al., 2017a)		
Carbonized mushrooms	78	1	Opten./Ecw.	(Xu et al., 2017a)		
Plasmonic wood	85	10	Opten./Alst.	(Tao et al., 2018a)		
Au nanoflowers/silica gel	85	1	Inwp.	(Gao et al., 2018)		
Au/Al ₂ O ₃ template	90	4	Opten./Alst.	(Zhou et al., 2016a)		
Au NPs/filter paper	89	10	Ecw.	(Liu et al., 2017f)		
Ink-stained paper	85.8	1	Ecw.	(Tao et al., 2018a)		
Ag/diatomite/airlaid paper	92.2	1	Opten./Ecw.	(Fang et al., 2017)		
Al NPs/AAM	88.4/91	4/6	Opten./Alst.	(Zhou et al., 2016b)		
Carbon NPs coated PVDF membrane	74.6	1.3	Pmd	(Wu et al., 2017a)		
Dye modified PTFE membranes	60	1	Pmd	(Fujiwara and Kikuchi, 2017		
Cone shaped PPy	93.8	1	Opten.	(Wang et al., 2018a)		
TiO ₂ -PDA/PPy/cotton	98	1	Ecw.	(Hao et al., 2018)		
TiAlON nanocomposite/NiO disk	73/90	1/4	Ecw.	(Liu et al., 2017c)		

^a Ecw.: External confined water path, Opten.: Optically enhanced, Inwp.: Internal water path, Alst.: Aligned structure, Pmd: Photothermal membrane distillation

5.1.1. OD or Nanosphere Structure

For 0D device structure, colloidal or nanosphere-based photothermal is dispersed in the water. Where the optical nanoparticles or nanofluids are homogenously dispersed all over the liquid and demonstrate moving heat generation through bulk water (Otanicar et al., 2010), hence, they can achieve limited conversion efficiency (Figure 10a) (Ni et al., 2015). Though it reduces surface heat losses, it still suffers from bulk water heating. Moreover, compact dispersion and continuous pumping of nanoparticles to the interior of the liquid under long-term irradiation remain challenging (Yu et al., 2017).

5.1.2. 1D or Linear Structure

A 1D pathway device was designed and fabricated by Li *et al.* to keep minimal heat loss in bulk water. They designed an umbrella-shaped absorber suspended in the air with a 1D pathway stand (Figure 10b&c). This 1D pathway serves water transportation along with minimal conduction, convection, and radiation losses. The umbrella-shaped absorber reduces the angular dependency of the light absorption and successfully gives STE efficiency of 85% (Li *et al.*, 2017b). To get improved efficiency in 1D design, Li *et al.* 3D printed 1D graphene oxide (GO) pillars suspended on a polystyrene insulator. This jellyfish-like evaporator demonstrates 87.5% efficiency under one sun illumination (Li *et al.*, 2017c).

5.1.3. 2D or Planar Structure

In another study, Li *et al.* engineered a 2D pathway to confine the water transport simultaneously and suppress bulk heat loss (Figure 10h-k) (Li et al., 2016a). They wrapped 2D cellulose paper on a PS-based

thermal insulator foam (thermal conductivity $\sim 0.04 W m^{-1} K^{-1}$) to enable non-stop water supply to the top GO absorber layer. The GO film is placed above the PS thermal insulator without direct contact with bulk water, significantly suppressing parasitic heat losses. This specially engineered 2D water supply exhibits 80% STE conversion efficiency under one sun illumination.

5.1.4. 3D or Bulk Structure

Most STE devices are interfacial 3D types, where a 3D structured device is floated or suspended in water. The 3D device must be specially configured and engineered to ensure a non-stop water supply and minimal heat loss. Maximum wettability and wicking capability, macro-or micro-porous enable, and minimal thermal conductivity are vital factors considered during 3D device design. Liu *et al.* have fabricated an artificial tree-like 3D device by carbonizing natural tree wood. This carbonized 3D device has enough porous structure with interconnected micro-/nanochannels to transport proper water to the hot zone (Figure 10d-g). The adequate water transportation, thermal management, and high light absorption in this tree-like 3D device give 89% STE efficiency under ten sun illumination (Liu et al., 2018a).

5.2. Bio-Inspired Device Structure

The biological body, predominantly plants, has a multi-channeled xylem-phloem tissue bundle that supports the transportation of water, food, and nutrients from roots to leaves. This complex tissue bundle possesses excellent hydrophilicity and minimal thermal conductivity,

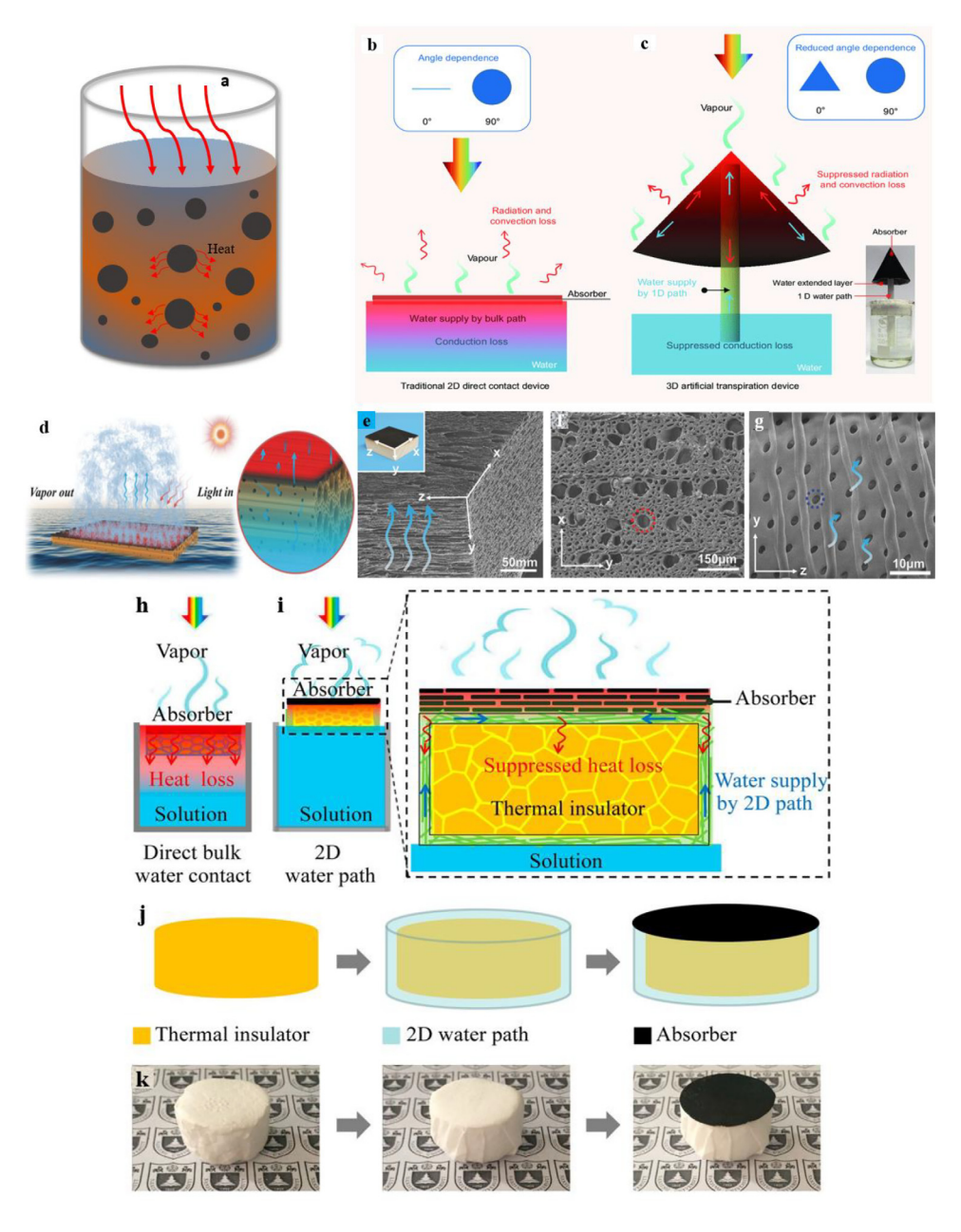


Figure 10. 0D, 1D, 2D, and 3D pathway device structure. a. 0D structure with uniformly dispersed nanoparticles in bulk water. b-c. schematics of conventional and 1D pathway devices. Images reproduced with the permission of ref. (Li et al., 2017b). d-g. 3D interfacial device structure with horizontally placed porosity and SEM images of the absorber. Images reproduced with the permission of ref. (Liu et al., 2018a). h-k. 2D water pathway design (wrapping thermal insulator) to confine the water transport. h. conventional evaporator. i. 2D enabled evaporator. j. fabrication processes of GO absorber with 2D wrapped path. k. physical photographs of arrangement of GO films with 2D wrapped water path. Images reproduced with the permission of ref. (Li et al., 2016a).

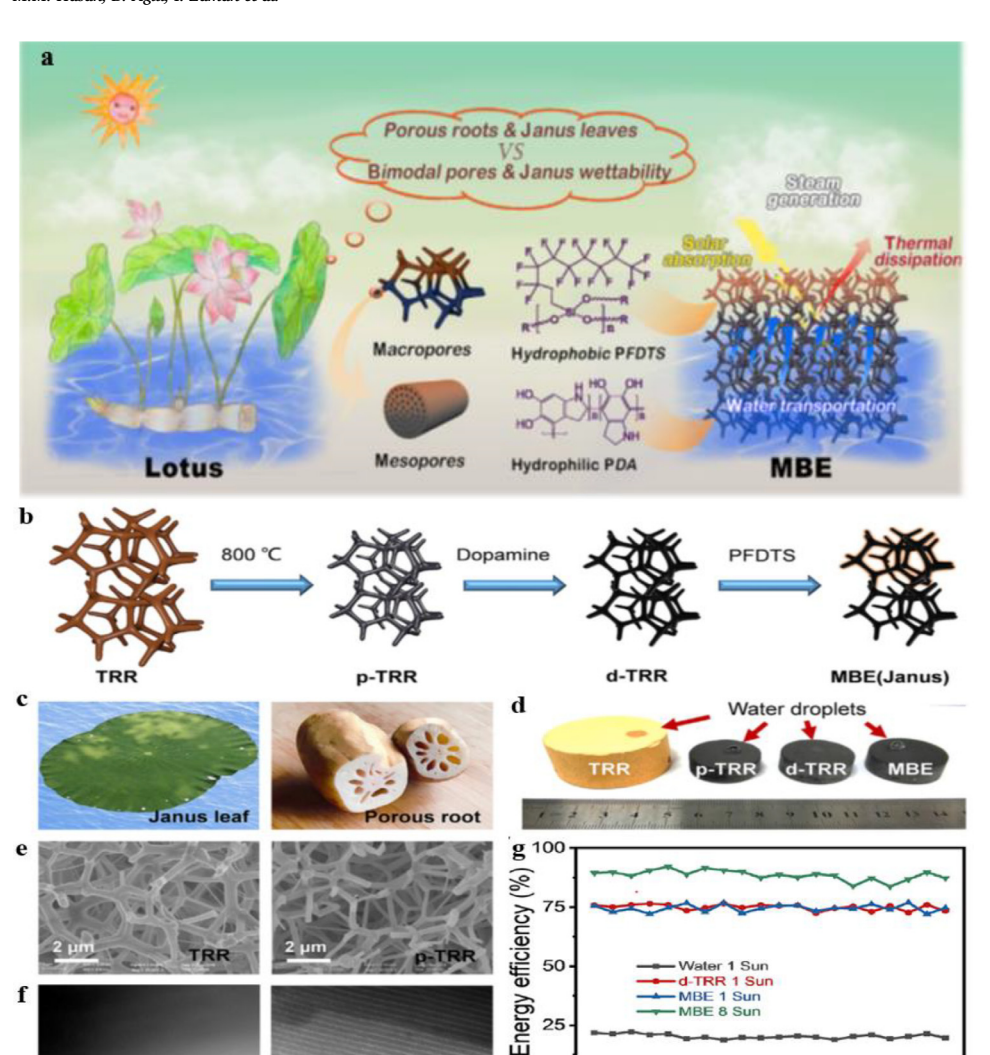
beneficial features for the STE mechanism. Researchers are mimicking this bio-inspired structure by designing various device configurations for high-performance STE.

Zhu *et al.* mimicked xylem-phloem multi-channel capillarity based on tree-inspired design. The top surface of longitudinal basswood is carbonized to develop an amorphous thin carbon layer that would serve as an absorber to mimic the tree-inspired design (Zhu *et al.*, 2017). Due to their excellent hydrophilicity, xylem-phloem bundle stacks under the carbon layer ensure continuous water transportation. Moreover, this non-carbonized substrate has very low thermal conductivity ($\sim 0.2Wm^{-1}K^{-1}$) (Song *et al.*, 2018), facilitating reduced thermal losses and improved STE efficiency by 87%. Zhang *et al.* mimicked the natural wood's internal structure with a xylem-phloem channel utilizing CNT to articulate channel orientation to fabricate an artificial hybrid wood evaporator (Zhang *et al.*, 2022). This artificial wood evaporator shows water-wicking flexibility with the enhanced solar-thermal property. To improve overall efficiency on wood-based STE devices, some

researchers exploited a variety of coatings, such as GO, CNT, graphite, and plasmonic nanoparticles (Chen et al., 2017b).

In some recent studies, along with wood, plant leaves (Geng et al., 2019), roots, mushrooms (Xu et al., 2017a), lotus (Zhao et al., 2020b), bamboos (Bian et al., 2019), carrot (Long et al., 2019), and grass (Wang et al., 2017c) inspired devices are also investigated with promising STE performances. Zhao et al. designed an evaporator mimicking lotus morphology, named morphology-inspired bio-mimetic evaporator (MBE), with Janus-type wettability and bio-modal pores for high-performance STE conversion (Figure 11a-g) (Zhao et al., 2020b). Mimicking Lotus leaves, the upper hydrophobic surface of MBE, prevents water capillarity in the air, enabling better salt rejection and high light absorption. On the other hand, the bottom hydrophilic d-TRR (truss-like resorcinol-formaldehyde resin) provides a faster water supply due to capillarity. MBE's bimodal-macropore structures effectively decrease the materials' density and thermal conductivity for self-floating and thermal regulation, respectively. This lotus-inspired MBE device demonstrates

f



50

25

p-TRR

Water 1 Sun d-TRR 1 Sun MBE 1 Sun MBE 8 Sun

10

Cycles

15

Figure 11. Lotus morphology-inspired bio-mimetic evaporator (MBE) system. a. Schematic demonstration of MBE system. b, chemical fabrication of MBE absorber, c. photographs of Janus leaf and root of Lotus. d. photographs of TRR, p-TRR, d-TRR, and MBE (up layer is f-TRR). e. SEM images of TRR (left) and p-TRR (right) demonstrate the macropore variation. f. TEM images of TRR (left) and p-TRR (right) show mesopore formation. g. the stability performances of MBE-based solar-thermal evaporation, with each cycle duration one hour. Images reproduced with the permission of ref. (Zhao et al., 2020b).

low thermal conductivity ($\sim 0.12W m^{-1} K^{-1}$) and high STE conversion efficiency (~90.5% under eight sun illumination).

Bian group carbonized a longitudinal bamboo trunk with a hierarchical cellular structure (Bian et al., 2019). The innermost wall of the bamboo trunk prevents light diffusion and radiative loss, and the outer wall absorbs thermal energy from the surroundings. The inner cellular mesh confines the water, which reduces the evaporation enthalpy. Attributed to all the above features, the 3D carbonized bamboo owns 132% STE conversion efficiency, resulting from the recovers of diffused energy from the inner wall, radiative loss at the bottom, and heat gain from a warmer environment. Long et al. fabricated ethanol-treated carrot biochar (ECB) (Long et al., 2019). ECB's distributed high porous channel enables uninterrupted water transport to the hot zone. It demonstrates 127.8% STE conversion efficiency, resulting from the reabsorbing diffused energy that reheats and accelerates evaporation. Some other bioinspired evaporators include but are not limited to bamboo stems, vegetable foams, loofah sponge, pomelo peel, willow catskins, algae, etc. (Fillet et al., 2021).

6. Applications of Solar-Thermal Evaporation Systems

Owing to its attractive features such as ease of fabrication, simple design, low-cost materials, renewable resources, long-term durability and stability, and eco-friendliness, the STE system has gained great attraction to adopt in various fields like electrical power generation, seawater desalination, wastewater purification, and hydrogen fuel production.

6.1. STE System Based Power Generation Techniques

20

Rotating the turbines requires high temperature and pressure in steam-assisted power generation systems. Low energy solar-thermal conversion can produce only low-temperature vapor under ambient pressure. This vapor has insufficient energy to rotate the gas turbines; thus, electricity production through conventional generators is unlikely. Recently, it has been reported that the solar-thermal system can generate high-temperature steam with convenient pressures under intense solar intensities. Sajadi et al. produced hot steam at 156 degrees celsius and 525 kPa pressures under 50 sun illuminations (Sajadi et al., 2016). They employed exfoliated porous graphite on the silicone skeleton with the support of aluminum foam to make the device thermally stable and prevent dry-out under high temperatures.

Theoretical calculation and simulation show that interfacial solarthermal evaporation could harness electrical power to such an extent that it will outcast all conventional power generations. This could happen because over 50% of solar power is directly absorbed by the earth's water surface and consequently lost as thermal energy. Cavusoglu et al. theoretically developed a relation between evaporation rate and power of STE-based system. They calculated the available power from the STE

engine floating on the water surface. In a case study, they chose the total water surface of United States reservoirs (excluding the Great Lakes) and calculated the obtainable power is nearly 325 GW which is over 69% of the United States' total power generation in 2015 (Cavusoglu et al., 2017). They also explored these lakes as an energy reservoirs due to the excellent heat capacity of water. They found that this thermal energy storage could help reduce volatility and intermittency of the power supply. This study indicates that since only some lakes can harness 325 GW of power, the vast sea surface could produce energy to an almost unimaginable extent.

To support the STE-based power generation concept, Xue et al. theoretically showed and experimentally proved that water's channel flow can induce stream-assisted potential. A natural porous carbon-based STE device can utilize this water channel flow and generate potential up to 1V lasting more than 480 hours (Xue et al., 2017c, Ding et al., 2017). However, since most solar power has been utilized by vapor generation, the solar-electricity conversion efficiency is low. These bi-functional characteristics of the STE system can be employed in low-power electronics, such as sensors and pyroelectric-nanogenerators (Gao et al., 2016).

6.1.1. Salinity Gradient-Based Power Generation

Solar-thermal evaporation could also produce electricity directly by exploiting the salinity gradient in the liquid. In terms of "blue energy," saline water contains more renewable energy than freshwater. This energy can be extracted and utilized in everyday life during the mixture of salty and freshwater. Theoretically, salinity gradient-based energy can be evaluated by the Gibbs free energy, ΔG_{max}

$$\Delta G_{\text{max}} = \text{RT} \left[c_{\text{m}} \ln(c_{\text{m}}) - \chi c_{\text{s}} \ln(c_{\text{s}}) - (1 - \chi) c_{\text{r}} \ln(c_{\text{r}}) \right]$$
 (5)

where χ is the fractional value of seawater, c_m is the concentration of the mixture, c_s is seawater concentration, and c_r is the freshwater concentration. Practically, the energy extracted from the system is always less than $\Delta G_{\rm max}$ since inevitable entropy is always associated. Reverse electro-dialysis, pressure retardation osmosis, and electric double-layer capacitor (EDLC) are the most common technologies to harvest this salinity-assisted energy from seawater. In reverse electro-dialysis, the chemically induced potential gradient separates charges across ion-exchange membranes and produces electricity. Pressure retarded osmosis utilizes salt-rejecting membranes to introduce an osmotic pressure between the two liquids to generate electrical energy. In EDLC, the alternative potential has resulted from alternating porous electrodes in different electrolytes of different salinity.

To harvest salinity-based potential, Yang et al. fabricated the two-layer device, a CNT-based layer on the top side and an ionselective membrane on the bottom side, and performed STE conversion (Yang et al., 2017). They reported that the rapid evaporation of water through the CNT-sheet leaves a salinity gradient in the bulk liquid, which assists the directional transport of the salt ions (Figure 12a). Seawater is continuously pumped to the "hot zone" due to the capillarity, producing vapor under illumination. A salinity gradient develops between ion-selective membranes after the rapid evaporation, which introduces a directional charge transport between layers. The experimental report shows it can generate electrical power around $1Wm^{-2}$ with a 75% efficiency of STE conversion. Based on the Gibbs theory, the energy production from the system can reach up to 12.5 Wm^{-2} . In this work, the obtained power is below 10% since the membrane hinders the positive and negative ions. This group also developed a scalable device to verify their ideas further. The experimental study shows after scaling, the evaporation rate can reach $1.1kgm^{-2}h^{-1}$. In addition, the open-circuit voltage V_{oc} is ~66 mV, and enhanced power of 3 mW can be achieved under a steady-state condition. Another group also exploited porous carbon films to produce electrical power from solar thermal evaporation (STE) (Xue et al., 2017d). The device is fabricated from carbon black films and consists of two CNT-based electrodes, which produce a reliable voltage of around 1.0 V under one sun illumination. The STE-driven water molecules interact with carbon atoms through redox and leave free electrons responsible for the potential difference between the upper and lower ends of the carbon film.

6.1.2. Electrostatic Power Generation

A triboelectric nanogenerator utilizes electrification or electrostatic effect and harvests mechanical energy (Wang et al., 2015). In electrification contact, two materials accumulate opposite charges due to friction, which results in triboelectric-based potential difference (Fan et al., 2012). While on-off contact between two materials periodically distributes the electrostatic charges and hence develops a potential difference. Frictional electrification introduces static triboelectric potential, while the electrostatic effect transforms mechanical energy into electrical energy (Niu and Wang, 2015). The induced potential V can be written as $\rho d/\varepsilon_0$. where ρ is the charge density, ε_0 is the vacuum permittivity, and d is the space between two layer. In both cases, the charge accumulates in two materials in a capacitive way; the external current flow can be written as,

$$I = V \frac{\partial C}{\partial t} + C \frac{\partial V}{\partial t} \tag{6}$$

where, C denotes the capacitance of materials, and V is the developed potential between layers(Lee et al., 2016).

Gao et al. recently developed a hybrid system for simultaneous water evaporation and triboelectricity generation (Gao et al., 2018). They fabricated an inexpensive 3D plasmonic absorber dispersed with gold nanoflowers (AuFs) in a silica substrate. The plasmonic characteristic of AuFs contributes to broadband absorption and high STE performance. The better heat confinement of silica-gel facilitates 85% STE conversion efficiency during one sun irradiation with $1.356\ kgm^{-2}h^{-1}$ evaporation rate. In this hybrid system, polytetrafluoroethylene (PTFE) produces voltage and current due to flow-induced electrification (Figure 12b). However, this device can obtain a little, but the optimized power is $0.6\mu W$.

6.1.3. Piezoelectric Power Generation

Stress-induced mechanical deformation can generate electricity via the piezoelectric effect. After exerting mechanical strain, the resulting deformation causes charge separation into the material. In that case, the charge density due to the piezoelectric effect can be evaluated as $\rho=dX$, where ρ is the charge density, d is the piezoelectric constant, and X is the applied strain. This induced electric field can be written as $\nabla E=\rho/E$ where, ε is the medium permittivity.

Mechanical deformation occurs through the structure upon heating or cooling, leading to charge separation and potential difference. Zhu et al. integrated a hybrid device to harvest piezoelectric and pyroelectric energy forms to utilize extra thermal energy during evaporation (Zhu et al., 2018d). They fabricated a carbon sponge with high absorptance and heat localization properties for in situ solar thermal evaporation. They have reported that the evaporation rate is 1.30 $kgm^{-2}h^{-1}$, with an STE conversion efficiency of 85%. They integrated the PVDF tweezer with an evaporator to harvest thermomechanical energy from steam turbulence (Figure 12c). PVDF shows outstanding piezo-pyroelectric properties with temperature oscillation and up-down fluctuation, producing electricity due to the piezoelectric effect. Under PVDF oscillation, the short-circuit current, I_{sc} and open-circuit voltage, V_{oc} could reach -0.08 μ A and -20.0 V, respectively.

6.1.4. Thermoelectric Power Generation

Seebeck's effect demonstrates that thermoelectric (TE) devices exploit spatial thermal gradients and substantially produce electrical power. Thermal to electrical via a thermoelectric device employing thermal gradients has gained tremendous attraction for real-time applications. People believe the thermoelectric effect is the best way to handle waste heat (Bell, 2008). Recent works on heat to electricity demonstrate that thermoelectric devices are promising for solar heat to electricity under concentrated conditions and STE at ambient temperature.

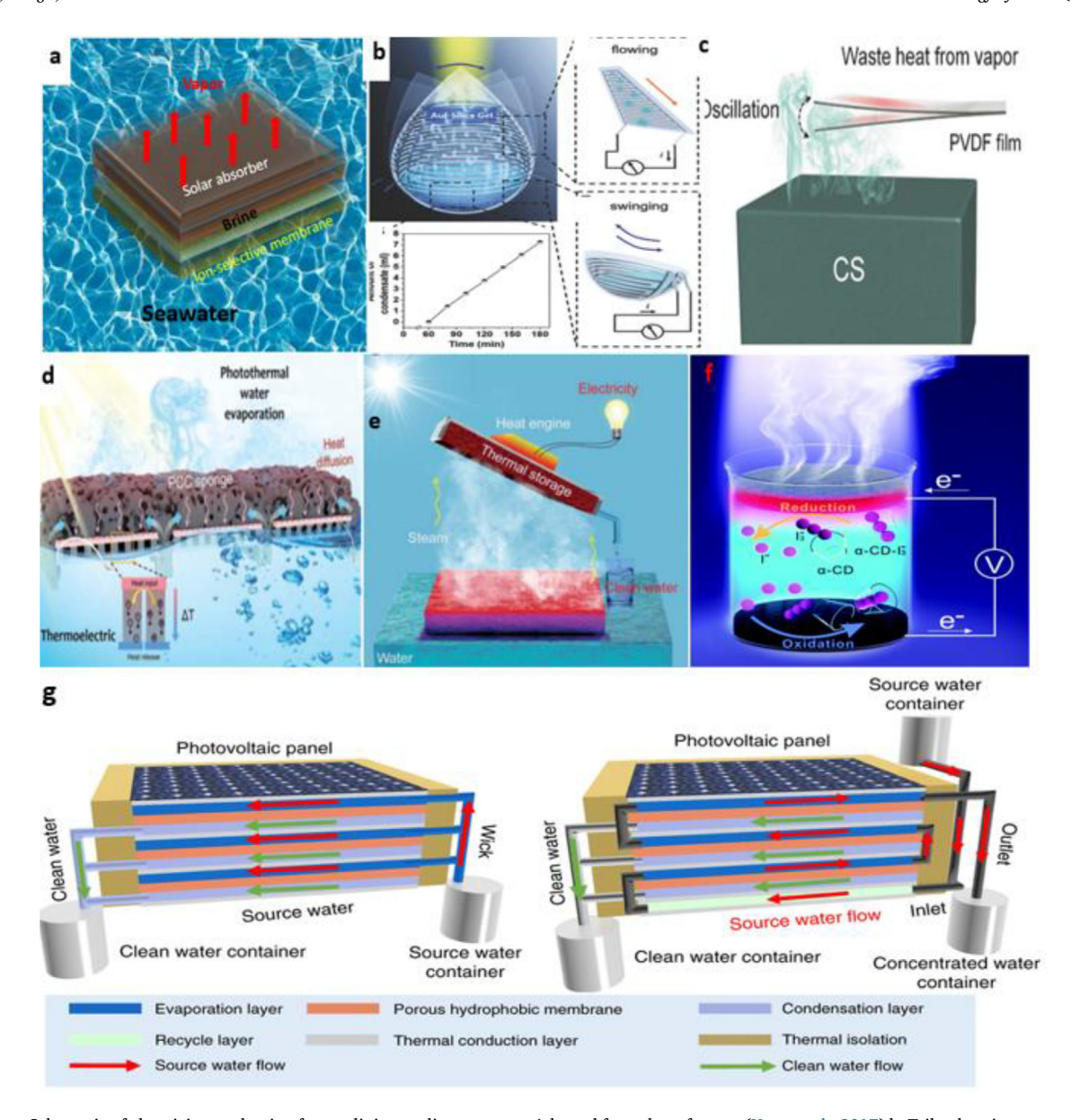


Figure 12. a. Schematic of electricity production from salinity gradient concept. Adopted from the reference (Yang et al., 2017) b. Triboelectric nanogenerator-based power generation from STE. Reproduced with the permission of ref. (Gao et al., 2018). c. thermal-induced piezoelectric effect in STE system to produce electricity. Reproduced with the consent of ref (Zhu et al., 2018d) d &e. Thermoelectric-based power extraction from STE hybrid system. Reproduced with the permission of ref. (Zhu et al., 2019) and (Li et al., 2018c). f. illustration of thermo-electrochemical conversion to generate power from the STE system. Reproduced with the approval of ref. (Shen et al., 2019). g. Multi-stage photovoltaic-membrane distillation system for freshwater and electricity co-generation. Image reproduced with the permission of ref. (Wang et al., 2019).

Zhu *et al.* manufactured a TE module integrated with the evaporator to harvest thermal energy (Zhu et al., 2019). Their experiment inserted a solar sponge between the TE module and the water and found the evaporation rate to be $1.36\ kgm^{-2}h^{-1}$ at one sun irradiation (Figure 12d). During the rapid evaporation, the temperature gradient between the hot zone and below the TE module incorporates a high TE-induced potential of 106 mV under one sun irradiation. The steam-assisted enthalpy during STE can be extracted by the TE module (Li et al., 2018c). Li *et al.* used a graphite-based evaporator in the STE system (Figure 12e). The broadband absorption capability and excellent thermal management enable a high evaporation rate of 34.8 $kgm^{-2}h^{-1}$, with an efficiency of 81.7% under 30-sun. The TE module attached to the evaporator can generate electrical power of 574mW with an efficiency of 1.23%. Cao *et al.* integrated a CNT foam/polyvinyl alcohol-based evaporator with a TE module. Their device architecture can potentially co-generate freshwa-

ter and electrical power under solar irradiation with the output power density of 0.4 Wm^{-2} and evaporation rate 5.0 $kgm^{-2}h^{-1}$ (Cao et al., 2021).

6.1.5. Electrochemical Power Generation

On the other hand, a thermo-electrochemical cell utilizes a temperature-dependent redox reaction to transform heat into electricity. A temperature gradient is introduced during the redox reaction at both the anode and cathode. The charge separation during redox in electrodes continuously produces electricity in the thermo-cell.

Incorporating the thermo-electrochemical concept in STE, Shen *et al.* utilized low-cost graphene-based electrodes in the STE system to further STE efficiency along with electrical power generation. This Graphite film electrodes also serve as a solar absorber (Shen et al., 2019). Under sunlight exposure, the temperature difference across the electrodes

develops a voltage difference due to the positive and negative charges separation (Figure 12f). During the experiment with seawater, the evaporation rate reached up to 1.1 $kgm^{-2}h^{-1}$ With an STE efficiency of 60%. The power generation was about 0.5 mWm^{-2} under solar irradiation. They also found that this thermo-electrochemical system can produce 0.023 mWm^{-2} even at night conditions due to infrared radiation.

6.1.6. Photovoltaic-Membrane Distillation Co-generation

Several groups have investigated how to simultaneously co-generate freshwater and photovoltaic power to address the water-energy nexus intimately. Wang et al. integrated a PV panel with a membrane distillation (PV-MD) (Wang et al., 2019) to co-generate freshwater and electricity from the sea, lake, or pond surface. They installed a multistage membrane distillation (MSMD) under the PV panel to utilize the 80-90% thermal losses during the photovoltaic conversion (Figure 12g). The evaporator of MSMD collected this thermal waste, and the vapor was generated utilizing this thermal waste. During an experiment with 3stage PV-MD, they found water production rate is 1.79 kgm⁻¹h⁻¹ under one sun illumination. The energy efficiency of 3 stage PV module was 11%. This work demonstrates that PV-MD integration could be an intelligent solution to the water-energy nexus. Especially in coastal areas, the floating PV-MD system could co-generate an accountable amount of freshwater and electrical power. This PV-MD generated power could feed the central grid-like other conventional PV systems.

6.2. Towards Off-grid and Microgrid Integration of STE Powered Systems (Futuristic View)

In a lot of practical applications, STE-generated power can be utilized efficiently. As discussed above, the output power density of a single STE module is pretty low. However, a matrix combination of series and parallel connections of m*n STE modules can multiply both voltage and current to the desired level to charge the off-grid storage systems such as batteries, supercapacitors, etc. (Dao et al., 2021). This enhanced power can also directly be used to power up several electronic devices such as LED bulbs, LCD monitors, IoTs, resistive switching memory, etc.

Practically, series or parallel combinations of desired numbers of STE devices can effortlessly multiply the output voltage, current, and power. Ji et al. reported that the series and parallel combination of four STE devices could provide the open-circuit voltage V_{oc} upto 6.2 V and the short circuit current Jsc around 550 nA (Ji et al., 2019). Moreover, with the parallel combination, the short circuit current Jsc can be scaled up to 280, 400, and 550 nA, respectively. To scale up Voc up to 20 V, they connected eighteen devices in series combination. In another work, Xue et al. placed four CB-coated slide glasses in a series combination and obtained V_{oc} upto 4.8V under one sun illumination, which can turn on an LCD (Xue et al., 2017d).

6.2.1. STE Module-Based System

Though the electrical properties like current, voltage, and power generated from the STE are pretty low, the device's innovative material usage and intelligent engineering can enhance both vapor and power generation. Moreover, assembling an STE array-like PV array with series and parallel combinations can significantly improve the current and voltage to the desired extent, which can easily integrate into the off- or microgrid application (see Fig. 13 for the microgrid integration). Since the STE module can generate only DC power, a storage device like a battery, supercapacitor, etc., will feed into the power system. This storage system will store the obtained power from the STE module and provide it to the inverter to convert the DC to AC power. In the grid system (microor main grid), the transmission and utilization of electrical power occur in an AC manner. So it is necessary to convert the DC power from the STE module to the AC power with the same frequency and amplitude as the grid.

Unlike other renewable energy sources, like wind, tidal and photovoltaic (PV) systems, STE-based power generation could eliminate grid-

connected transmission and utilization uncertainty. The better prediction of power quality from STE sources happens due to thermal-assisted evaporation, which leaves a power generation footprint, even any sunlight fluctuations (Xue et al., 2017d). Solar radiation is highly intermittent and volatile, and an abrupt change in solar irradiation can occur (Notton and Voyant, 2018). Though transient in nature, the solar-assisted STE system will not shut down power generation immediately since there's still will be enough thermal energy to generate STE-based power to a certain extent.

In a conventional PV system, power generation failure occurs due to abrupt fluctuations of solar irradiation. Solar-based PV power generation largely depends on the availability of sunlight, irradiation intensity, and the duration of daytime. These are the function of unpredictable weather conditions and the sun's annual position, making the harnessed power volatile and intermittent (Figueiredo and Silva, 2019). The same thing happens in wind-based power sources. Wind power is more intermittent and volatile than solar energy. The power quality in wind systems largely depends on air quality and speed. Any airspeed randomness incorporates intermittency and volatility in power production (Jabir et al., 2017). Though tidal power harnessing is less volatile and intermittent than solar and wind, its variability is still a considerable concern during grid integration (Lewis et al., 2019). This intermittency and volatility of solar, wind, and tidal sources bring the sudden failure of power generation and consequent shutdown of the whole grid if there is no backup power generation or storage. In terms of dispatchability, STE-based integration is more dispatchable than solar, wind, and tidal power but less dispatchable than geothermal, hydropower and biomass. Dispatchability can be referred to as the ability of power sources to synchronize supply and demand as quickly as possible (Emmanuel and Rayudu, 2017).

In the modern power grid system, dispatchability plays a crucial role due to on-demand supply. The massive penetration of renewable power like photovoltaic, wind, and tidal in the grid system introduces nondispatchability due to intermittency and generation uncertainty (please see Table 2 for the comparative studies of variabilities of renewable power penetration without a storage system) (Gea, 2012). But unlike other renewable resources, the STE system-based power penetration is more dispatchable and would be a more favorable source to the grid. This happens since STE-based power harnessing is less volatile and intermittent by nature. A complex control mechanism needs to be integrated with the grid system to address these problems (volatility, intermittency, and non-dispatchability in solar and wind power generation) and for continuous power supply to the utilities. But in an STE-based source, the abrupt failure of the system is controllable since the power generation will not shut down immediately due to its thermal dependence functionality. Hence, the grid will have enough time to adjust the demand and supply with a less complex control mechanism. In addition, solar and wind power systems require a lot of financial budgets and land space to install and maintain.

On the other hand, STE power systems do not need substantial economic costs and land space since they can be installed on the open sea surface, and the STE device follows low-cost materials and fabrication. Though pros over PV and wind sources to some extent, the STE integration requires a lot of water surface and enough sunlight. Since the photovoltaic system can easily do solar to electrical conversion with better efficiency, the PV system will outcast standalone STE-based power generation. Moreover, standalone STE-based power generation is not economical. Still, hybrid integration of clean water production and power generation can solve the water power scarcity in some under-developed coastal areas.

6.2.2. STE Vapor Insertion in the Steam Turbine System

The new research focuses on combining solar thermal evaporation and steam turbine, and the STE vapor could be inserted in the steam chamber to lump up more steam. STE produces vapor with low temperature and pressure to rotate the turbine. So, inserting STE vapor in the

Wind anergy

VSI

Wind Supervisory Control

Solar PV

VSI

Wind Supervisory Control

PCC

Utility grid

Hydropower

Figure 13. Schematic illustration of STE module integration (red circled) to micro-grid systems

Table 2
Comparative variable characteristics of renewable energy resources and emerging STE sources. Data are collected from the following references: (Gea, 2012), (Bessa et al., 2014), (Chen et al., 2019b), (Figueiredo and Silva, 2019), (Lewis et al., 2019), (Emmanuel and Rayudu, 2017), and (Ruiz et al., 2013).

Renewable Resources Characteristics of RES	Photovoltaic	Wind	STE System	Geothermal	Hydropower	Biomass	Tidal
Volatility	High	High	Mild	Low	Low	Low	Mild
Intermittency	High	High	Mild	Low	Low	Low	Mild
Uncertainty	High	High	Mild	Low	Low	Low	Mild
Dispatchability	Low	Low	Mild	High	High	High	Low

steam chamber will lump up the total steam, where low-temperature vapor will gain enough energy due to the excessive heat in the chamber and directly associate with accumulating high-energy steam. This conceptual hybrid system can use concentrated solar energy, biofuel, or geothermal energy as a primary heat source. The low-energy steam needs to be dumped in a sink for the complete thermal cycle. The sink could be a water reservoir like ponds, rivers, or oceans. This wastage heat could then be reused to produce freshwater using thermal-based evaporation (Figure 14). This two-fold usage of the systems will enable freshwater production and enhanced steam-assisted power generation. This manifold hybrid system is the crucial concept of a synergy city, which can confront major issues like freshwater production where drinkable water is scarce, green power production, and safe disposal of waste heat to the reservoir (Crespo Del Granado et al., 2016).

6.3. Other Applications of STE Systems

6.3.1. Desalination

In recent years, freshwater scarcity has been a significant concern for social welfare and people's health regarding pressing drinking water. Around 66% of the earth's population, approximately four billion, currently live under the scarcity line for at least one month a year (Mekonnen and Hoekstra, 2016). This picture will be much scarier by 2040 due to the ever-growing population, agricultural farms, and industries (Figure 1b) (Neto, 2018). To meet the projected demands, it is

inevitable to increase the freshwater production from various resources like the sea, river, lake, contaminated reservoirs, etc. Using conventional technologies to produce mass freshwater faces high capital costs and low conversion efficiency, hindering expectations. Recent inventions of high absorptive photothermal materials and smart systems engineering revive solar-thermal evaporation with high efficiency but low capital costs. Desalination has commonly been named a process in which potable water is extracted from saline water. Seawater, a vast saline water source, could be a ground space for desalination. In the natural desalination process, seawater is heated by sunlight and creates vapor. However, the pretty slow evaporation rate and low efficiency due to low absorption and volumetric losses limit the practical applications for potable water production. Recently, smart engineering of solar-thermal devices with very high absorptive materials minimized thermal losses. Proper vapor escape has opened a new road to producing drinkable water through desalination. In this process, enough vapor is generated by the solar-thermal device. The as-produced vapor act as a thermal energy carrier and can be converted to water by the old-fashioned cooling process. Since the vapor is a low-temperature phase below boiling point, a straightforward way to cool down is by utilizing cold or normal air (Figure 15a) (Li et al., 2018b). Continuous capillary water pumping to the evaporative zone completes the cycle and continuous-rapid pure water generation. Compared with conventional freshwater production such as thermal distillation and reverse osmosis process, the solar-thermal evaporation STE systems employ simple device design and infrastruc-

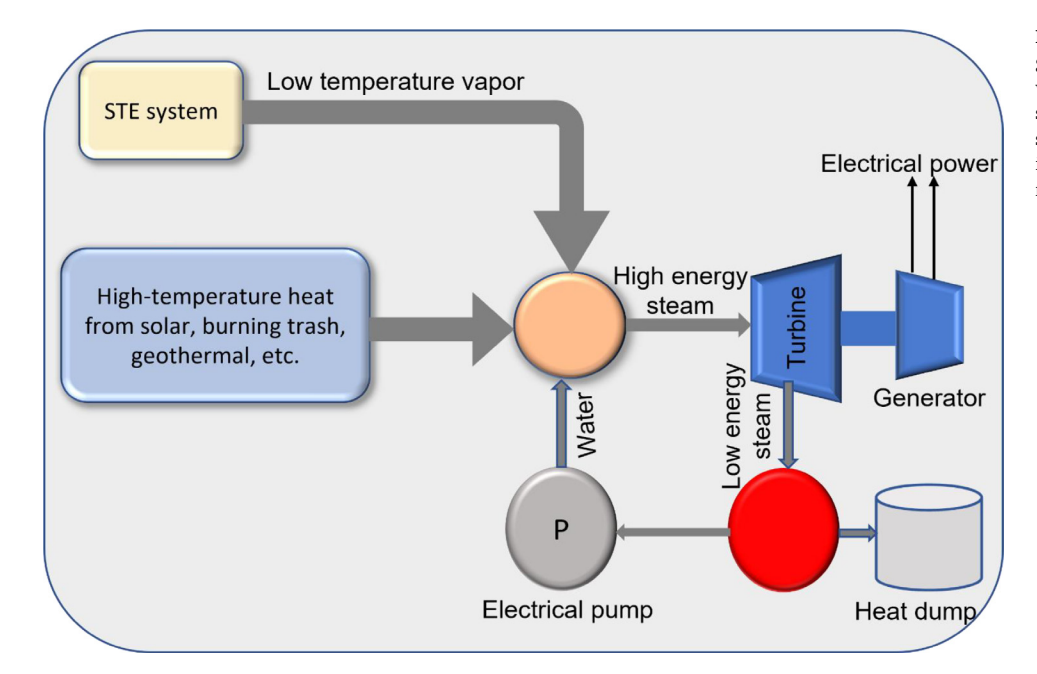


Figure 14. Conceptual illustration of STE integration in synergy city power generation. Low vapor has been integrated with high-energy steam to increase the internal volume and pressure. This integration will increase the torque in the turbine, hence more electrical power from the generator.

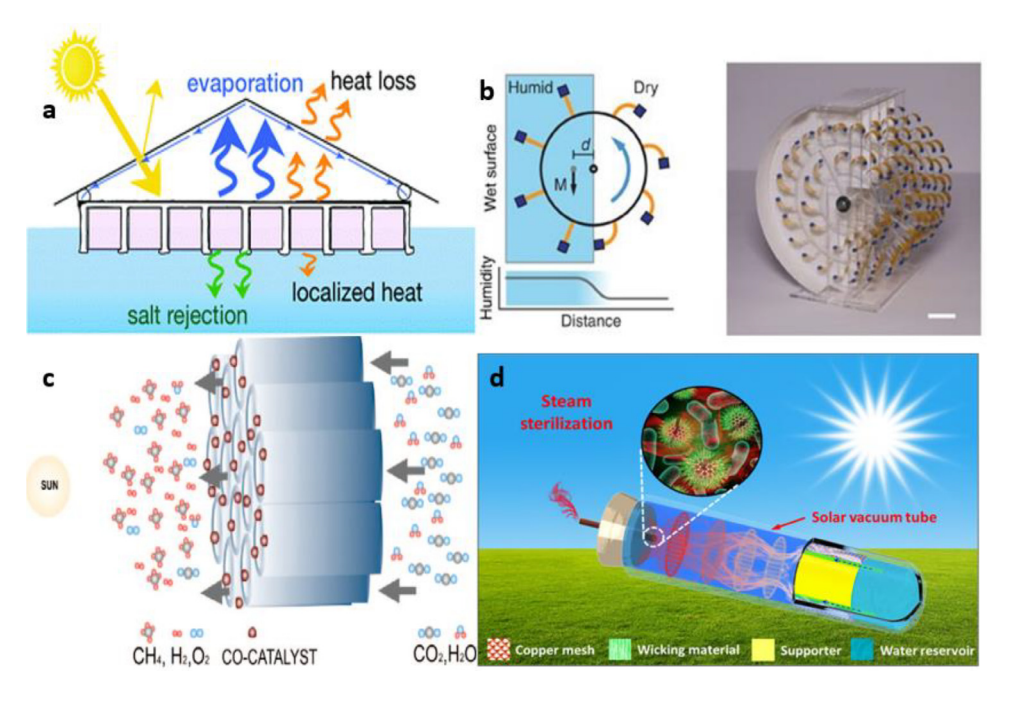


Figure 15. Illustrations of some practical applications of solar-driven evaporation systems. a. Pure water production scheme from saline water. Image reproduced with the permission of ref. (Ni et al., 2018). b. Harvesting of mechanical energy employing humidity gradient to rotate the moisture mill. Image reproduced with the permission of ref. (Chen et al., 2015). c. Schematic of solar-chemical hydrogen fuel production. Image reproduced with the approval of ref. (Varghese et al., 2009). d. Schematic of STE-enabled sterilization system. Image reproduced with the permission of ref. (Chang et al., 2019).

ture, hence do not require an external power source to pump the water and complex treatment equipment (Khawaji et al., 2008).

Currently, a small-scale STE system can produce 2.5 liters per square meter of square water on a typical sunny day, which is enough for a single person daily (Ni et al., 2018). Owing to low-cost design and infrastructure, solar-driven evaporation system installation costs only US\$3 $\rm m^{-2}Which$ is ten times lower than the old-fashioned solar still system. Recent literature shows that solar-thermal conversion can also exploit solar-driven photocatalytic degradation (Lou et al., 2016). Solar-thermal evaporation enhances the photocatalytic reaction due to elevated temperature and diffusion of reactants accelerated by the vapor flow.

6.3.2. Mechanical and Chemical Energy Extraction

The STE system has also opened possibilities to convert solar energy to mechanical and chemical energy. Chen *et al.* placed a moisture

mill above the evaporator to create a significant humidity contrast to investigate the effect of humidity gradient on mechanics (Chen et al., 2015). In their arrangement, half of the mill film is within the humid region, and the rest half of it is in the dry air. Half-film's humid area is coated with moisture-sensitive spores, which can straighten under a humidity gradient. The other half-film in the dry air can bend due to a lack of humidity. This type of asymmetry assisted by evaporation causes the mass to shift to the center, and eventually, the rotation occurs (Figure 15b). The solar thermochemical and photocatalytic processes can produce hydrogen fuel. In this process, the hot vapor is mixed with methane hydrocarbon or other biomasses with catalysts (Nakajima et al., 2016). The photothermal device produces hot vapor, so a vapor-methanol reforming reaction occurs. As a byproduct, hydrogen production happens in this reaction, and since hydrogen is lighter than air and vapor, it can rapidly be removed from the evaporation area (Figure 15c).

6.3.3. Sterilization

Superheated steam is one of the best approaches to sterilizing water, medical equipment, food containers, etc. In this method, superheated steam (typically above 100°C) is traditionally produced by an electric heater and then applied to kill the bacterial, fungal, or virus contamination. In many undeveloped areas, electricity is scarce, which lacks traditional sterilization methods (Pittet et al., 2008). STE-enabled hightemperature vapor could become an economical and green solution for sterilization in these areas. To efficiently enable STE-based sterilization, Deng et al. proposed and fabricated an rGO/polytetrafluoroethylene composite membrane absorber that can localize the heat in the hot zone. This localized heat produces superheated vapor (above 120°C), demonstrating successful chemical and biological sterilization under normal conditions (Zhang et al., 2017c). In another work, this group manufactured a portable vacuum tube integrated with an STE device to commercialize the STE-enabled sterilization concept (Chang et al., 2019). This mobile device can generate superheated vapor under normal conditions and shows excellent sterilization for biological indicators and bacterial pathogens (Figure 15d). Using the carbonization method, another group fabricated a biochar-based autoclave absorber from the banana peel, orange peel, fallen leaves, bamboo, and tree branches. After the fabrication, they performed the STE experiment to produce superheated vapor (above 121°C) to support the sterilization techniques. Their experiment found effective sterilization with 99.99999% killing of the pathogen (Li et al., 2018a). The previous discussion shows that STE-enabled sterilization can provide the best possible solution for sterilizing water, medical equipment, food containers, etc., where traditional electricity-based sterilizer is scarce.

7. Discussion and Perspectives

Last few years, solar-thermal evaporation has been extensively explored through orchestrated endeavors from diverse disciplines. Though the attempt to integrate the STE system with commerce is early, the clear demonstration of efficient vapor generation and utilization in various sectors such as electrical power generation, clean water production, sterilization, and photo catalyzation has enabled this novel device to become a next-generation state-of-art technology. Moreover, it does not need complex infrastructures, electrical circuitry, expensive materials, or human resources. Along with these features, it is also environment-friendly and cost-effective, which makes it a sustainable and economically viable solution for electricity generation and freshwater production.

However, several issues need to be addressed in STE systems for commercialization and comprehensive utilization. First of all, develop standardized performance analysis techniques. The lack of standard measurement and calculation hinders the comparison between various findings. The best possible solution could be establishing a specific mathematical model and defining state-of-the-art parameters. Moreover, it is necessary to acknowledge the natural evaporation rate during STE conversion to state the influence of the environment.

During evaporator fabrication, ultra-high light absorptive materials must be chosen with excellent stability and durability under wet conditions. The blackbody emissions further impair the performances of the devices, so it is necessary to coat the devices with IR films or utilize novel materials as an evaporator with very high absorption but very low emission. Radiative losses in the surroundings are another concerning issue in the case of high efficiency. To minimize losses, anti-reflection films may need to be coated at the air-evaporator interface. Conduction and convection losses in bulk water are central to the total loss. These losses must need to be minimized as much as possible. Very high thermal insulators must be placed between the water and the evaporator. In the case of designing a thermal insulator, the wettability and hydrophilicity attribute needs to be assured for proper and sufficient water transport. Vapor escape is another issue for efficient vapor generation and removal. Without proper vapor escape, the as-generated va-

por can block the sunlight from entering the evaporator, reducing the photo-thermal conversion.

Moreover, since the as-generated vapor has a low-temperature state, it can conglomerate and dramatically change the phase to water and eventually drop to the evaporator surface, impeding the overall vapor production and power generation. Stability and durability under thermal and wet conditions are other important issues that must be adequately addressed. Unstable devices can degrade under extreme temperature and liquid, which questions long-term durability and would not be economically viable. The impacts of humidity and pressure also need to be studied since lower moisture and higher pressure enhance vapor generation. Therefore, an intelligent choice of innovative materials and proper device engineering with these critical features would enable the solar-thermal evaporator in large-scale commercialization.

In the case of power generation, some critical issues need to be addressed appropriately. First of all, the trade-off between evaporation rate and power generation. During vapor and power generation synergy, absorbed light energy is split into two systems (neglecting losses). Some portion creates vapor, and the rest of them harness the power. So a considerable trade-off between evaporation and power generation needs to be established. Moreover, the light-vapor-electricity hybrid STE system stability is another issue that must be managed adequately. Various factors like absorber materials, humidity, air, water temperature, and salinity accumulation over the absorber surface significantly affect the system's stability. These factors must be managed smartly to enhance synergy performances.

So far, the obtained output power from STE systems is pretty low and can merely be used as a single power source. To enhance the output power to the desired level, the multiple STE devices need to be arrayed to make a floating STE module (like a PV array module). This module can potentially increase the voltage and current to the desired level. The floating module should be placed above the seawater so that the system would be cleaner, environmentally friendly, and have zero toxicity in the sea ecosystem. Since the power generation from STE largely depends on the availability of sunlight, it is highly intermittent. Due to the intermittent nature, integrating into the grid system would be challenging without any robust control system. Finally, the device must be configured intelligently to maximize power and freshwater production.

8. Conclusion

Freshwater production and electricity generation are two major challenges for modern life and must be managed intelligently. Nowadays, freshwater generation consumes a lot of electrical power. On the other hand, most conventional power plants necessitate tons of freshwater. So, the generation of these two has consuming effects on one another. Solar-thermal evaporation STE is the first technology in human history that can generate both freshwater and electricity without consuming one another. Moreover, this system is renewable, eco-friendly, and has zero footprints on the environment. If commercialized, the STE system would be a next-generation state-of-the-art technology to address the rising demand for fresh water and electrical power. Though the STE system is still in laboratories, soon, it will become a great help to eliminate water scarcity and illuminate the world with electricity, especially in coastal areas. However, several issues must be tackled innovatively. STE device configuration still needs to be improved on the central issues, such as the appropriate absorptive materials, innovative device structure, and efficient vapor collection. Moreover, a reasonable efficiency trade-off must be scaled and adjusted during freshwater and power cogeneration. Soon, if all the current issues are adequately addressed and adjusted, the solar-thermal evaporation system will be a next-generation clean energy system to nexus freshwater and power generation.

By harnessing the sun's plentiful energy, STE-based studies hope to provide both electricity and fresh water. In the scientific communities, this study has been acknowledged via several benchmark review evaluations over the last few years. Upon closer inspection, it becomes clear that most review papers treat particular elements of STE systems, such as absorber materials, the physics and chemistry of the STE system, the architecture of the device, desalination, and purification, power production, etc., in isolation. However, there has been minimal effort to analyze all of these topics in one place comprehensively. This article addresses the aforementioned knowledge gap by thoroughly discussing solar thermal evaporation's physics, chemistry, and engineering using the most up-to-date research available. It also provides a comprehensive presentation of the many fascinating uses for STE systems, including the production of power from renewable sources and the synergy idea. The unique and practical presentation of physics, chemistry, device design engineering, power generation, and microgrid integration makes this review both novel and useful. This study intends to provide a comprehensive analysis of recent developments in STE systems to encourage primary and practical research in the utilization of underutilized supplemental energy sources for the future integration of water, energy, and environmental systems with the potential for research advancement.

Conflict of interest

The authors declare no conflicts of interest.

Data availability

Data will be made available on request.

References

- Angel, N., Vijayaraghavan, S.N., Yan, F., Kong, L., 2020. Electrospun Cadmium Selenide Nanoparticles-Loaded Cellulose Acetate Fibers for Solar Thermal Application. Nanomaterials 10, 1329.
- Banat, F., Jwaied, N., Rommel, M., Koschikowski, J., Wieghaus, M., 2007. Desalination by a "compact SMADES" autonomous solarpowered membrane distillation unit. Desalination 217, 29–37.
- Bell, L.E., 2008. Cooling, Heating, Generating Power, and Recovering Waste Heat with Thermoelectric Systems. Science 321, 1457–1461.
- Bessa, R., Moreira, C., Silva, B., Matos, M., 2014. Handling renewable energy variability and uncertainty in power systems operation. WIREs Energy and Environment 3, 156–178.
- Bian, Y., Du, Q., Tang, K., Shen, Y., Hao, L., Zhou, D., Wang, X., Xu, Z., Zhang, H., Zhao, L., Zhu, S., Ye, J., Lu, H., Yang, Y., Zhang, R., Zheng, Y., Gu, S., 2019. Carbonized Bamboos as Excellent 3D Solar Vapor-Generation Devices. Advanced Materials Technologies 4, 1800593.
- Bian, Y., Tang, K., Xu, Z., Ma, J., Shen, Y., Hao, L., Chen, X., Nie, K., Li, J., Ma, T., Zhu, S., Ye, J., Xiong, X., Yang, Y., Zhang, R., Zheng, Y., Gu, S., 2018. Highly efficient solar steam generation by hybrid plasmonic structured TiN/mesoporous anodized alumina membrane. Journal of Materials Research 33, 3857–3869.
- Blanco, J., Malato, S., Fernandez-Ibanez, P., Alarcón, D., Gernjak, W., Maldonado, M, 2009. Review of feasible solar energy applications to water processes.
- Brongersma, M.L., Halas, N.J., Nordlander, P., 2015. Plasmon-induced hot carrier science and technology. Nat Nanotechnol 10, 25–34.
- Cai, J., Qi, L., 2015. Recent advances in antireflective surfaces based on nanostructure arrays. Materials Horizons 2, 37–53.
- Cao, F., Kraemer, D., Tang, L., Li, Y., Litvinchuk, A.P., Bao, J., Chen, G., Ren, Z., 2015. A high-performance spectrally-selective solar absorber based on a yttria-stabilized zirconia cermet with high-temperature stability. Energy & Environmental Science 8, 3040–3048.
- Cao, P., Zhao, L., Yang, Z., Yuan, P., Zhang, Y., Li, Q., 2021. Carbon Nanotube Network-Based Solar-Thermal Water Evaporator and Thermoelectric Module for Electricity Generation. ACS Applied Nano Materials 4, 8906–8912.
- Cavusoglu, A.-H., Chen, X., Gentine, P., Sahin, O., 2017. Potential for natural evaporation as a reliable renewable energy resource. Nature Communications 8, 617.
- Chang, C., Tao, P., Xu, J., Fu, B., Song, C., Wu, J., Shang, W., Deng, T., 2019. High-Efficiency Superheated Steam Generation for Portable Sterilization under Ambient Pressure and Low Solar Flux. ACS Applied Materials & Interfaces 11, 18466–18474.
- Chen, C., Kuang, Y., Hu, L., 2019a. Challenges and Opportunities for Solar Evaporation. Joule 3, 683–718.
- Chen, C., Li, Y., Song, J., Yang, Z., Kuang, Y., Hitz, E., Jia, C., Gong, A., Jiang, F., Zhu, J.Y., Yang, B., Xie, J., Hu, L., 2017a. Highly Flexible and Efficient Solar Steam Generation Device. Adv Mater 29.
- Chen, C., Li, Y., Song, J., Yang, Z., Kuang, Y., Hitz, E., Jia, C., Gong, A., Jiang, F., Zhu, J.Y., Yang, B., Xie, J., Hu, L., 2017b. Highly Flexible and Efficient Solar Steam Generation Device. Advanced Materials 29, 1701756.
- Chen, M., He, Y., Huang, J., Zhu, J., 2016. Synthesis and solar photo-thermal conversion of Au, Ag, and Au-Ag blended plasmonic nanoparticles. Energy Conversion and Management 293–300.
- Chen, Q., Pei, Z., Xu, Y., Li, Z., Yang, Y., Wei, Y., Ji, Y., 2018. A durable monolithic polymer foam for efficient solar steam generation. Chem Sci 9, 623–628.

- Chen, R., Wu, Z., Zhang, T., Yu, T., Ye, M., 2017c. Magnetically recyclable self-assembled thin films for highly efficient water evaporation by interfacial solar heating. RSC Advances 7, 19849–19855.
- Chen, S., Fang, G., Huang, X., Yan, M., 2019b. A joint optimal dispatching method of wind-solar-hydro generation system. IOP Conference Series: Earth and Environmental Science 227, 032004.
- Chen, X., Goodnight, D., Gao, Z., Cavusoglu, A.H., Sabharwal, N., Delay, M., Driks, A., Sahin, O., 2015. Scaling up nanoscale water-driven energy conversion into evaporation-driven engines and generators. Nat Commun 6, 7346.
- Chen, X., Liu, L., Yu, P.Y., Mao, S.S., 2011. Increasing solar absorption for photocatalysis with black hydrogenated titanium dioxide nanocrystals. Science 331, 746–750.
- Chen, Y., Zhao, X., Ye, Z., Chen, Y., Lin, P., 2022. Robust seawater desalination and sewage purification enabled by the solar-thermal conversion of the Janus-type graphene oxide evaporator. Desalination 522, 115406.
- Chen, Z., Chen, M., Yan, H., Zhou, P., Chen, X., 2020. Enhanced solar thermal conversion performance of plasmonic gold dimer nanofluids. Applied Thermal Engineering 178, 115561.
- Chou, J.B., Yeng, Y.X., Lee, Y.E., Lenert, A., Rinnerbauer, V., Celanovic, I., Soljačić, M., Fang, N.X., Wang, E.N., Kim, S.-G, 2014. Enabling Ideal Selective Solar Absorption with 2D Metallic Dielectric Photonic Crystals. Advanced Materials 26, 8041–8045.
- Crespo Del Granado, P., Pang, Z., Wallace, S., 2016. Synergy of smart grids and hybrid distributed generation on the value of energy storage. Applied Energy 170, 476–488.
- Dao, V.-D., Choi, H.-S., 2018. Carbon-Based Sunlight Absorbers in Solar-Driven Steam Generation Devices. Global Challenges 2, 1700094.
- Dao, V.-D., Vu, N.H., Thi Dang, H.-L., Yun, S, 2021. Recent advances and challenges for water evaporation-induced electricity toward applications. Nano Energy 85, 105979.
- Deng, Z., Zhou, J., Miao, L., Liu, C., Peng, Y., Sun, L., Tanemura, S., 2017. The emergence of solar thermal utilization: solar-driven steam generation. Journal of Materials Chemistry A 5, 7691–7709.
- Ding, T., Liu, K., Li, J., Xue, G., Chen, Q., Huang, L., Hu, B., Zhou, J., 2017. All-Printed Porous Carbon Film for Electricity Generation from Evaporation-Driven Water Flow. Advanced Functional Materials 27, 1700551.
- Ding, T., Zhou, Y., Ong, W.L., Ho, G.W., 2021. Hybrid solar-driven interfacial evaporation systems: Beyond water production towards high solar energy utilization. Materials Today 42, 178–191.
- Dongare, P.D., Alabastri, A., Pedersen, S., Zodrow, K.R., Hogan, N.J., Neumann, O., Wu, J., Wang, T., Deshmukh, A., Elimelech, M., Li, Q., Nordlander, P., Halas, N.J., 2017. Nanophotonics-enabled solar membrane distillation for off-grid water purification. Proceedings of the National Academy of Sciences 114, 6936–6941.
- El-Sayed, M.A., 2001. Some Interesting Properties of Metals Confined in Time and Nanometer Space of Different Shapes. Accounts of Chemical Research 34, 257–264.
- Emmanuel, M., Rayudu, R., 2017. Evolution of dispatchable photovoltaic system integration with the electric power network for smart grid applications: A review. Renewable and Sustainable Energy Reviews 67, 207–224.
- Fan, F.-R., Tian, Z.-Q., Lin Wang, Z., 2012. Flexible triboelectric generator. Nano Energy 1, 328–334.
- Fang, J., Liu, Q., Zhang, W., Gu, J., Su, Y., Su, H., Guo, C., Zhang, D., 2017. Ag/diatomite for highly efficient solar vapor generation under one-sun irradiation. Journal of Materials Chemistry A 5, 17817–17821.
- Figueiredo, N.C., Silva, P.P.D., 2019. The "Merit-order effect" of wind and solar power: Volatility and determinants. Renewable and Sustainable Energy Reviews 102, 54–62.
- Fillet, R., Nicolas, V., Fierro, V., Celzard, A., 2021. A review of natural materials for solar evaporation. Solar Energy Materials and Solar Cells 219, 110814.
- Fridleifsson, I.B., 2001. Geothermal energy for the benefit of the people. Renewable and Sustainable Energy Reviews 5, 299–312.
- Fu, Y., Wang, G., Mei, T., Li, J., Wang, J., Wang, X., 2017. Accessible Graphene Aerogel for Efficiently Harvesting Solar Energy. ACS Sustainable Chemistry & Engineering 5, 4665–4671
- Fujiwara, M., Kikuchi, M., 2017. Solar desalination of seawater using double-dye-modified PTFE membrane. Water Research 127, 96–103.
- Gao, F., Li, W., Wang, X., Fang, X., Ma, M., 2016. A self-sustaining pyroelectric nanogenerator driven by water vapor. Nano Energy 22, 19–26.
- Gao, M., Peh, C.K., Phan, H.T., Zhu, L., Ho, G.W., 2018. Solar Absorber Gel: Localized Macro-Nano Heat Channeling for Efficient Plasmonic Au Nanoflowers Photothermic Vaporization and Triboelectric Generation. Advanced Energy Materials 8, 1800711.
- Gao, M., Zhu, L., Peh, C.K., Ho, G.W., 2019. Solar absorber material and system designs for photothermal water vaporization towards clean water and energy production. Energy & Environmental Science 12, 841–864.
- Gao, X., Ren, H., Zhou, J., Du, R., Yin, C., Liu, R., Peng, H., Tong, L., Liu, Z., Zhang, J., 2017. Synthesis of Hierarchical Graphdiyne-Based Architecture for Efficient Solar Steam Generation. Chemistry of Materials 29, 5777–5781.
- García-Vidal, F.J., Pitarke, J.M., Pendry, J.B, 1997. Effective Medium Theory of the Optical Properties of Aligned Carbon Nanotubes. Physical Review Letters 78, 4289–4292.
- GEA, 2012. Global Energy Assessment Toward a Sustainable Future. Cambridge University Press, Cambridge, UK and New York, NY, USA and the International Institute for Applied Systems Analysis, Laxenburg, Austria.
- Geng, H., Xu, Q., Wu, M., Ma, H., Zhang, P., Gao, T., Qu, L., Ma, T., Li, C., 2019. Plant leaves inspired sunlight-driven purifier for high-efficiency clean water production. Nature Communications 10, 1512.
- Ghasemi, H., Ni, G., Marconnet, A.M., Loomis, J., Yerci, S., Miljkovic, N., Chen, G., 2014. Solar steam generation by heat localization. Nat Commun 5, 4449.
- Gong, B., Yang, H., Wu, S., Tian, Y., Yan, J., Cen, K., Bo, Z., Ostrikov, K., 2022. Nanotexturing-enhanced heat transfer and interfacial evaporation for energy-efficient solar-thermal water desalination. International Journal of Heat and Mass Transfer 186, 122462.

- Goto, K., Yogo, K. & Higashii, T. 2013. A review of efficiency penalty in a coal-fired power plant with post-combustion CO2 capture.
- Guo, A., Ming, X., Fu, Y., Wang, G., Wang, X., 2017. Fiber-Based, Double-Sided, Reduced Graphene Oxide Films for Efficient Solar Vapor Generation. ACS Applied Materials & Interfaces 9, 29958–29964.
- Hao, D., Yang, Y., Xu, B., Cai, Z., 2018. Bifunctional Fabric with Photothermal Effect and Photocatalysis for Highly Efficient Clean Water Generation. ACS Sustainable Chemistry & Engineering 6, 10789–10797.
- He, S., Chen, C., Kuang, Y., Mi, R., Liu, Y., Pei, Y., Kong, W., Gan, W., Xie, H., Hitz, E., Jia, C., Chen, X., Gong, A., Liao, J., Li, J., Ren, Z.J., Yang, B., Das, S., Hu, L., 2019. Nature-inspired salt resistant bimodal porous solar evaporator for efficient and stable water desalination. Energy & Environmental Science 12, 1558–1567.
- Higgins, M.W., Shakeel Rahmaan, A.R., Devarapalli, R.R., Shelke, M.V., Jha, N., 2018. Carbon fabric based solar steam generation for waste water treatment. Solar Energy 159, 800–810
- Homola, J., 2003. Present and future of surface plasmon resonance biosensors. Analytical and Bioanalytical Chemistry 377, 528–539.
- Hordy, N., Coulombe, S., Meunier, J.-L., 2013. Plasma Functionalization of Carbon Nanotubes for the Synthesis of Stable Aqueous Nanofluids and Poly(vinyl alcohol) Nanocomposites. Plasma Processes and Polymers 10, 110–118.
- Hordy, N., Rabilloud, D., Meunier, J.-L., Coulombe, S., 2014. High temperature and long-term stability of carbon nanotube nanofluids for direct absorption solar thermal collectors. Solar Energy 105, 82–90.
- Hua, Z., LI, B., LI, L., Yin, X., Chen, K., Wang, W., 2017. Designing a Novel Photothermal Material of Hierarchical Microstructured Copper Phosphate for Solar Evaporation Enhancement. The Journal of Physical Chemistry C 121, 60–69.
- Huang, C.-H., Huang, J.-X., Chiao, Y.-H., Chang, C.-M., Hung, W.-S., Lue, S.J., Wang, C.-F., Hu, C.-C., Lee, K.-R., Pan, H.-H., Lai, J.-Y., 2021. Tailoring of a Piezo-Photo-Thermal Solar Evaporator for Simultaneous Steam and Power Generation. Advanced Functional Materials 31, 2010422.
- Huang, X., Yu, Y.-H., De, LLERGO, Oscar, L., Marquez, S.M., Cheng, Z, 2017. Facile polypyrrole thin film coating on polypropylene membrane for efficient solar-driven interfacial water evaporation. RSC Advances 7, 9495–9499.
- Huang, Z.F., Song, J., Li, K., Tahir, M., Wang, Y.T., Pan, L., Wang, L., Zhang, X., Zou, J.J., 2016. Hollow Cobalt-Based Bimetallic Sulfide Polyhedra for Efficient All-pH-Value Electrochemical and Photocatalytic Hydrogen Evolution. J Am Chem Soc 138, 1359–1365.
- Ishii, S., Sugavaneshwar, R.P., Nagao, T., 2016. Titanium Nitride Nanoparticles as Plasmonic Solar Heat Transducers. The Journal of Physical Chemistry C 120, 2343–2348.
- Ito, Y., Tanabe, Y., Han, J., Fujita, T., Tanigaki, K., Chen, M., 2015a. Multifunctional Porous Graphene for High-Efficiency Steam Generation by Heat Localization. Advanced Materials 27, 4302–4307.
- Ito, Y., Tanabe, Y., Han, J., Fujita, T., Tanigaki, K., Chen, M., 2015b. Multifunctional Porous Graphene for High-Efficiency Steam Generation by Heat Localization. Adv Mater 27, 4302–4307.
- Ito, Y., Tanabe, Y., Sugawara, K., Koshino, M., Takahashi, T., Tanigaki, K., Aoki, H., Chen, M., 2017. Three-dimensional porous graphene networks expand graphene-based electronic device applications. Physical Chemistry Chemical Physics 20
- Jabir, M., Azil Illias, H., Raza, S., Mokhlis, H., 2017. Intermittent Smoothing Approaches for Wind Power Output: A Review. Energies 10, 1572.
- Ji, B., Chen, N., Shao, C., Liu, Q., Gao, J., Xu, T., Cheng, H., Qu, L., 2019. Intelligent multiple-liquid evaporation power generation platform using distinctive Jaboticaba-like carbon nanosphere@TiO2 nanowires. Journal of Materials Chemistry A 7, 6766–6772.
- Jia, C., Li, Y., Yang, Z., Chen, G., Yao, Y., Jiang, F., Kuang, Y., Pastel, G., Xie, H., Yang, B., Das, S., Hu, L., 2017. Rich Mesostructures Derived from Natural Woods for Solar Steam Generation. Joule 1, 588–599.
- Jian, H., Wang, Y., Li, W., Ma, Y., Wang, W., Yu, D., 2021. Reduced graphene oxide aerogel with the dual-cross-linked framework for efficient solar steam evaporation. Colloids and Surfaces A: Physicochemical and Engineering Aspects 629, 127440.
- Jiang, Q., Gholami Derami, H., Ghim, D., Cao, S., Jun, Y.-S., Singamaneni, S., 2017. Poly-dopamine-filled bacterial nanocellulose as a biodegradable interfacial photothermal evaporator for highly efficient solar steam generation. Journal of Materials Chemistry A 5, 18397–18402.
- Jiang, R., Cheng, S., Shao, L., Ruan, Q., Wang, J., 2013. Mass-Based Photothermal Comparison Among Gold Nanocrystals, PbS Nanocrystals, Organic Dyes, and Carbon Black. The Journal of Physical Chemistry C 117, 8909–8915.
- Jin, X., Li, Y., Li, W., Zheng, Y., Fan, Z., Han, X., Wang, W., Lin, T., Zhu, Z., 2019. Nano-material Design for Efficient Solar-Driven Steam Generation. ACS Applied Energy Materials 2, 6112–6126.
- Kabeel, A.E., el-agouz, S.A., 2011. Review of researches and developments on solar stills. Desalination 276, 1–12.
- Kashyap, V., Ghasemi, H., 2020. Solar heat localization: concept and emerging applications. Journal of Materials Chemistry A 8, 7035–7065.
- Keshavarz Hedayati, M., Elbahri, M., 2016. Antireflective Coatings: Conventional Stacking Layers and Ultrathin Plasmonic Metasurfaces, A Mini-Review. Materials 9, 497.
- Khawaji, A.D., Kutubkhanah, I.K., Wie, J.-M., 2008. Advances in seawater desalination technologies. Desalination 221, 47–69.
- Kim, K., Yu, S., An, C., Kim, S.-W., Jang, J.-H., 2018. Mesoporous Three-Dimensional Graphene Networks for Highly Efficient Solar Desalination under 1 sun Illumination. ACS Applied Materials & Interfaces 10, 15602–15608.
- Kospa, D.A., Ahmed, A.I., Samra, S.E., Ibrahim, A.A., 2021. High efficiency solar desalination and dye retention of plasmonic/reduced graphene oxide based copper oxide nanocomposites. RSC Advances 11, 15184–15194.
- Lee, J.-H., Kim, J., Kim, T.Y., Al Hossain, M.S., Kim, S.-W., Kim, J.H., 2016. All-in-one energy harvesting and storage devices. Journal of Materials Chemistry A 4, 7983–7999.

- Lewis, M., Mcnaughton, J., Márquez-Dominguez, C., Todeschini, G., Togneri, M., Masters, I., Allmark, M., Stallard, T., Neill, S., Goward-Brown, A., Robins, P, 2019. Power variability of tidal-stream energy and implications for electricity supply. Energy 183, 1061–1074.
- Lewis, N.S., 2016. Research opportunities to advance solar energy utilization. Science 351, aad 1920.
- Li, J., Du, M., Lv, G., Zhou, L., Li, X., Bertoluzzi, L., Liu, C., Zhu, S., Zhu, J., 2018a. Interfacial Solar Steam Generation Enables Fast-Responsive, Energy-Efficient, and Low-Cost Off-Grid Sterilization. Advanced Materials 30, 1805159.
- Li, L., Feng, S., Du, L., Wang, Y., Ge, C., Yang, X., Wu, Y., Liu, M., Wang, S., Bai, Y., Sun, F., Zhang, T., 2022. A hydrovoltaic power generation system based on solar thermal conversion. Nano Energy 99, 107356.
- Li, R., Zhang, L., Shi, L., Wang, P., 2017a. MXene Ti3C2: An Effective 2D Light-to-Heat Conversion Material. ACS Nano 11, 3752–3759.
- Li, T., Liu, H., Zhao, X., Chen, G., Dai, J., Pastel, G., Jia, C., Chen, C., Hitz, E., Sid-dhartha, D., Yang, R., Hu, L., 2018b. Scalable and Highly Efficient Mesoporous Wood-Based Solar Steam Generation Device: Localized Heat, Rapid Water Transport. Advanced Functional Materials 28, 1707134.
- Li, W., Tian, X., Li, X., Han, S., Li, C., Zhai, X.-Z., Kang, Y., Yu, Z.-Z., 2021. Ultrahigh solar steam generation rate of a vertically aligned reduced graphene oxide foam realized by dynamic compression. Journal of Materials Chemistry A 9, 14859–14867.
- Li, X., Lin, R., Ni, G., Xu, N., Hu, X., Zhu, B., Lv, G., Li, J., Zhu, S., Zhu, J., 2017b. Three-dimensional artificial transpiration for efficient solar waste-water treatment. National Science Review 5, 70–77.
- Li, X., Min, X., Li, J., Xu, N., Zhu, P., Zhu, B., Zhu, S., Zhu, J., 2018c. Storage and Recycling of Interfacial Solar Steam Enthalpy. Joule 2, 2477–2484.
- Li, X., Xu, W., Tang, M., Zhou, L., Zhu, B., Zhu, S., Zhu, J., 2016a. Graphene oxide-based efficient and scalable solar desalination under one sun with a confined 2D water path. Proceedings of the National Academy of Sciences 113, 13953–13958.
- Li, X., Xu, W., Tang, M., Zhou, L., Zhu, B., Zhu, S., Zhu, J., 2016b. Graphene oxide-based efficient and scalable solar desalination under one sun with a confined 2D water path. Proc Natl Acad Sci U S A 113, 13953–13958.
- Li, Y., Gao, T., Yang, Z., Chen, C., Kuang, Y., Song, J., Jia, C., Hitz, E.M., Yang, B., Hu, L., 2017c. Graphene oxide-based evaporator with one-dimensional water transport enabling high-efficiency solar desalination. Nano Energy 41, 201–209.
- Li, Y., Gao, T., Yang, Z., Chen, C., Luo, W., Song, J., Hitz, E., Jia, C., Zhou, Y., Liu, B., Yang, B., Hu, L., 2017d. 3D-Printed, All-in-One Evaporator for High-Efficiency Solar Steam Generation under 1 Sun Illumination. Adv Mater 29.
- Lin, K.-T., Lin, H., Yang, T., Jia, B., 2020. Structured graphene metamaterial selective absorbers for high efficiency and omnidirectional solar thermal energy conversion. Nature Communications 11, 1389.
- Liu, C., Huang, J., Hsiung, C.-E., Tian, Y., Wang, J., Han, Y., Fratalocchi, A., 2017a. High-Performance Large-Scale Solar Steam Generation with Nanolayers of Reusable Biomimetic Nanoparticles. Advanced Sustainable Systems 1, 1600013.
- Liu, G., Chen, T., Xu, J., Li, G., Wang, K., 2020. Solar evaporation for simultaneous steam and power generation. Journal of Materials Chemistry A 8, 513–531.
- Liu, G., Xu, J., Wang, K., 2017b. Solar water evaporation by black photothermal sheets. Nano Energy 41, 269–284.
- Liu, H., Chen, C., Chen, G., Kuang, Y., Zhao, X., Song, J., Jia, C., Xu, X., Hitz, E., Xie, H., Wang, S., Jiang, F., Li, T., Li, Y., Gong, A., Yang, R., Das, S., Hu, L., 2018a. High-Performance Solar Steam Device with Layered Channels: Artificial Tree with a Reversed Design. Advanced Energy Materials 8, 1701616.
- Liu, H., Zhang, X., Hong, Z., Pu, Z., Yao, Q., Shi, J., Yang, G., Mi, B., Yang, B., Liu, X., Jiang, H., Hu, X., 2017c. A bioinspired capillary-driven pump for solar vapor generation. Nano Energy 42, 115–121.
- Liu, K.K., Jiang, Q., Tadepalli, S., Raliya, R., Biswas, P., Naik, R.R., Singamaneni, S., 2017d. Wood-Graphene Oxide Composite for Highly Efficient Solar Steam Generation and Desalination. ACS Appl Mater Interfaces 9, 7675–7681.
- Liu, P.-F., Miao, L., Deng, Z., Zhou, J., Su, H., Sun, L., Tanemura, S., Cao, W., Jiang, F., Zhao, L.-D., 2018b. A mimetic transpiration system for record high conversion efficiency in solar steam generator under one-sun. Materials Today Energy 8, 166–173.
- Liu, Y., Chen, J., Guo, D., Cao, M., Jiang, L., 2015. Floatable, Self-Cleaning, and Carbon-Black-Based Superhydrophobic Gauze for the Solar Evaporation Enhancement at the Air-Water Interface. ACS Appl Mater Interfaces 7, 13645–13652.
- Liu, Z., Song, H., Ji, D., Li, C., Cheney, A., Liu, Y., Zhang, N., Zeng, X., Chen, B., Gao, J., Li, Y., Liu, X., Aga, D., Jiang, S., Yu, Z., Gan, Q., 2017e. Extremely Cost-Effective and Efficient Solar Vapor Generation under Nonconcentrated Illumination Using Thermally Isolated Black Paper. Glob Chall 1, 1600003.
- Liu, Z., Yang, Z., Huang, X., Xuan, C., Xie, J., Fu, H., Wu, Q., Zhang, J., Zhou, X., Liu, Y., 2017f. High-absorption recyclable photothermal membranes used in a bionic system for high-efficiency solar desalination via enhanced localized heating. Journal of Materials Chemistry A 5, 20044–20052.
- Liz-Marzán, L.M, 2006. Tailoring Surface Plasmons through the Morphology and Assembly of Metal Nanoparticles. Langmuir 22, 32–41.
- Long, Y., Huang, S., Yi, H., Chen, J., Wu, J., Liao, Q., Liang, H., Cui, H., Ruan, S., Zeng, Y.-J., 2019. Carrot-inspired solar thermal evaporator. Journal of Materials Chemistry A 7, 26911–26916.
- Lou, J., Liu, Y., Wang, Z., Zhao, D., Song, C., Wu, J., Dasgupta, N., Zhang, W., Zhang, D., Tao, P., Shang, W., Deng, T., 2016. Bioinspired Multifunctional Paper-Based rGO Composites for Solar-Driven Clean Water Generation. ACS Appl Mater Interfaces 8, 14628–14636.
- Maier, S.A., Kik, P.G., Atwater, H.A., Meltzer, S., Harel, E., Koel, B.E., Requicha, A.A.G., 2003. Local detection of electromagnetic energy transport below the diffraction limit in metal nanoparticle plasmon waveguides. Nature Materials 2, 229–232.
- Margeson, M.J., Dasog, M., 2020. Plasmonic metal nitrides for solar-driven water evaporation. Environmental Science: Water Research & Technology 6, 3169–3177.

- Mekonnen, M.M., Hoekstra, A.Y., 2016. Four billion people facing severe water scarcity. Science Advances 2, e1500323.
- Nakajima, H., Lee, D., Lee, M.-T., Grigoropoulos, C.P., 2016. Hydrogen production with CuO/ZnO nanowire catalyst for a nanocatalytic solar thermal steam-methanol reformer. International Journal of Hydrogen Energy 41, 16927–16931.
- Neto, S., 2018. Territorial Integration of Water Management in the City. Water Challenges of an Urbanizing World.
- Ni, G., Li, G., Boriskina, S., Li, H., Yang, W., Zhang, T., Chen, G., 2016a. Steam generation under one sun enabled by a floating structure with thermal concentration. Nature Energy 1, 16126.
- Ni, G., Li, G., Boriskina, S.V., Li, H., Yang, W., Zhang, T., Chen, G., 2016b. Steam generation under one sun enabled by a floating structure with thermal concentration. Nature Energy 1.
- Ni, G., Miljkovic, N., Ghasemi, H., Huang, X., Boriskina, S.V., Lin, C.-T., Wang, J., Xu, Y., Rahman, M.M., Zhang, T., Chen, G., 2015. Volumetric solar heating of nanofluids for direct vapor generation. Nano Energy 17, 290–301.
- Ni, G., Zandavi, S.H., Javid, S.M., Boriskina, S.V., Cooper, T.A., Chen, G., 2018. A salt-rejecting floating solar still for low-cost desalination. Energy & Environmental Science 11, 1510–1519.
- Niu, S., Wang, Z.L., 2015. Theoretical systems of triboelectric nanogenerators. Nano Energy 14, 161–192.
- Notton, G., Voyant, C., 2018. Chapter 3 Forecasting of Intermittent Solar Energy Resource. In: YAHYAOUI, I. (Ed.), Advances in Renewable Energies and Power Technologies. Elsevier.
- Okumus, I., Dinler, A., 2016. Current status of wind energy forecasting and a hybrid method for hourly predictions. Energy Conversion and Management 123, 362–371.
- Oldenburg, S.J., Averitt, R.D., Westcott, S.L., Halas, N.J., 1998. Nanoengineering of optical resonances. Chemical Physics Letters 288, 243–247.
- Otanicar, T., Phelan, P., Prasher, R.S., Rosengarten, G., Taylor, R, 2010. Nanofluid-based direct absorption solar collector. Journal of Renewable and Sustainable Energy 2, 033102.
- Pang, Y., Zhang, J., Ma, R., Qu, Z., Lee, E., Luo, T., 2020. Solar–Thermal Water Evaporation: A Review. ACS Energy Letters 5, 437–456.

Peng, Q. & Qin, Y. 2011. ZnO Nanowires and Their Application for Solar Cells.

- Pittet, D., Allegranzi, B., Storr, J., Nejad, S.B., Dziekan, G., Leotsakos, A., Donaldson, L., 2008. Infection control as a major World Health Organization priority for developing countries. Journal of Hospital Infection 68, 285–292.
- Qiblawey, H.M., Banat, F., 2008. Solar thermal desalination technologies. Desalination 220, 633–644.
- Rahman, M.M., Younes, H., Ni, G., Lu, J.Y., Raza, A., Zhang, T.J., Fang, N.X., Ghaferi, A.A., 2017. Plasmonic nanofluids enhanced solar thermal transfer liquid. AIP Conference Proceedings 1850, 110013.
- Ren, H., Tang, M., Guan, B., Wang, K., Yang, J., Wang, F., Wang, M., Shan, J., Chen, Z., Wei, D., Peng, H., Liu, Z., 2017. Hierarchical Graphene Foam for Efficient Omnidirectional Solar–Thermal Energy Conversion. Advanced Materials 29, 1702590.
- Richardson, H.H., Carlson, M.T., Tandler, P.J., Hernandez, P., Govorov, A.O., 2009. Experimental and theoretical studies of light-to-heat conversion and collective heating effects in metal nanoparticle solutions. Nano Lett 9, 1139–1146.
- Ruiz, J.A., Juárez, M.C., Morales, M.P., Muñoz, P., Mendívil, M.A, 2013. Biomass gasification for electricity generation: Review of current technology barriers. Renewable and Sustainable Energy Reviews 18, 174–183.
- Rycenga, M., Cobley, C.M., Zeng, J., Li, W., Moran, C.H., Zhang, Q., Qin, D., Xia, Y., 2011. Controlling the synthesis and assembly of silver nanostructures for plasmonic applications. Chem Rev 111, 3669–3712.
- Sajadi, S.M., Farokhnia, N., Irajizad, P., Hasnain, M., Ghasemi, H., 2016. Flexible artificially-networked structure for ambient/high pressure solar steam generation. Journal of Materials Chemistry A 4, 4700–4705.
- Sattar, A., Farooq, M., Amjad, M., Saeed, M.A., Nawaz, S., Mujtaba, M.A., Anwar, S., El-Sherbeeny, A.M., Soudagar, M.E.M., Bandarra Filho, E.P., Ali, Q., Imran, M., Pettinau, A, 2020. Performance Evaluation of a Direct Absorption Collector for Solar Thermal Energy Conversion. Energies 13, 4956.
- Seh, Z.W., Liu, S., Low, M., Zhang, S.-Y., Liu, Z., Mlayah, A., Han, M.-Y., 2012. Janus Au– TiO2 Photocatalysts with Strong Localization of Plasmonic Near-Fields for Efficient Visible-Light Hydrogen Generation. Advanced Materials 24, 2310–2314.
- Shan, Y., Yao, G., Xu, J., Liu, G., 2021. Solar thermal evaporation using bubbly nanofluids with recyclable magnetic particles. Materials Today Communications 26, 102084.
- Shen, Q., Ning, Z., Fu, B., Ma, S., Wang, Z., Shu, L., Zhang, L., Wang, X., Xu, J., Tao, P., Song, C., Wu, J., Deng, T., Shang, W., 2019. An open thermo-electrochemical cell enabled by interfacial evaporation. Journal of Materials Chemistry A 7, 6514–6521.
- Shi, L., Wang, X., Hu, Y., He, Y., Yan, Y., 2020. Solar-thermal conversion and steam generation: a review. Applied Thermal Engineering 179, 115691.
- Shi, L., Wang, Y., Zhang, L., Wang, P., 2017. Rational design of a bi-layered reduced graphene oxide film on polystyrene foam for solar-driven interfacial water evaporation. Journal of Materials Chemistry A 5, 16212–16219.
- Shi, Y., Li, R., Jin, Y., Zhuo, S., Shi, L., Chang, J., Hong, S., Ng, K.-C., Wang, P., 2018a. A 3D Photothermal Structure toward Improved Energy Efficiency in Solar Steam Generation. Joule.
- Shi, Y., Li, R., Shi, L., Ahmed, E., Jin, Y., Wang, P., 2018b. A Robust CuCr2O4/SiO2 Composite Photothermal Material with Underwater Black Property and Extremely High Thermal Stability for Solar-Driven Water Evaporation. Advanced Sustainable Systems 2, 1700145.
- Song, J., Chen, C., Zhu, S., Zhu, M., Dai, J., Ray, U., Li, Y., Kuang, Y., Li, Y., Quispe, N., Yao, Y., Gong, A., Leiste, U.H., Bruck, H.A., Zhu, J.Y., Vellore, A., Li, H., Minus, M.L., Jia, Z., Martini, A., Li, T., Hu, L., 2018. Processing bulk natural wood into a high-performance structural material. Nature 554, 224–228.

- Soo Joo, B., Soo Kim, I., Ki Han, I., Ko, H., Gu Kang, J., Kang, G, 2022. Plasmonic silicon nanowires for enhanced heat localization and interfacial solar steam generation. Applied Surface Science 583. 152563.
- Steinfeld, A., 2005. Solar thermochemical production of hydrogen—a review. Solar Energy 78, 603–615.
- Sun, W., Zhong, G., Kübel, C., Jelle, A.A., Qian, C., Wang, L., Ebrahimi, M., Reyes, L.M., Helmy, A.S., Ozin, G.A, 2017. Size-Tunable Photothermal Germanium Nanocrystals. Angewandte Chemie International Edition 56, 6329–6334.
- Tang, Y., Zeng, X., Liang, J., 2010. Surface Plasmon Resonance: An Introduction to a Surface Spectroscopy Technique. Journal of chemical education 87, 742– 746.
- Tao, F., Zhang, Y., Yin, K., Cao, S., Chang, X., Lei, Y., Wang, D., Fan, R., Dong, L., Yin, Y., Chen, X., 2018a. A plasmonic interfacial evaporator for high-efficiency solar vapor generation. Sustainable Energy & Fuels 2, 2762–2769.
- Tao, P., Ni, G., Song, C., Shang, W., Wu, J., Zhu, J., Chen, G., Deng, T., 2018b. Solar-driven interfacial evaporation. Nature Energy 3, 1031–1041.
- Thirugnanasambandam, M., Iniyan, S., Goic, R., 2010. A review of solar thermal technologies. Renewable and Sustainable Energy Reviews 14, 312–322.
- Tina, G., Gagliano, S., Raiti, S., 2006. Hybrid solar/wind power system probabilistic modelling for long-term performance assessment. Solar Energy 80, 578–588.
- Tiwari, G., Singh, H., Tripathi, R., 2003. Present status of solar distillation. Solar Energy 75, 367–373.
- Ueno, K., Oshikiri, T., Sun, Q., Shi, X., Misawa, H., 2018. Solid-State Plasmonic Solar Cells. Chemical Reviews 118, 2955–2993.
- Uihlein, A., Magagna, D., 2016. Wave and tidal current energy A review of the current state of research beyond technology. Renewable and Sustainable Energy Reviews 58, 1070–1081.
- Umlauff, M., Hoffmann, J., Kalt, H., Langbein, W., Hvam, J.M., Scholl, M., Söllner, J., Heuken, M., Jobst, B., Hommel, D, 1998. Direct observation of free-exciton thermalization in quantum-well structures. Physical Review B 57, 1390–1393.
- Varghese, O.K., Paulose, M., Latempa, T.J., Grimes, C.A., 2009. High-Rate Solar Photocatalytic Conversion of CO2 and Water Vapor to Hydrocarbon Fuels. Nano Letters 9, 731–737.
- Vélez-Cordero, J.R., Hernández-Cordero, J, 2015. Heat generation and conduction in PDMS-carbon nanoparticle membranes irradiated with optical fibers. International Journal of Thermal Sciences 96, 12–22.
- Wang, G., Fu, Y., Guo, A., Mei, T., Wang, J., Li, J., Wang, X., 2017a. Reduced Graphene Oxide-Polyurethane Nanocomposite Foam as a Reusable Photoreceiver for Efficient Solar Steam Generation. Chemistry of Materials 29, 5629–5635.
- Wang, J., Li, Y., Deng, L., Wei, N., Weng, Y., Dong, S., Qi, D., Qiu, J., Chen, X., Wu, T., 2017b. High-Performance Photothermal Conversion of Narrow-Bandgap Ti2 O3 Nanoparticles. Adv Mater 29.
- Wang, P., 2018. Emerging investigator series: the rise of nano-enabled photothermal materials for water evaporation and clean water production by sunlight. Environmental Science: Nano 5, 1078–1089.
- Wang, W., Shi, Y., Zhang, C., Hong, S., Shi, L., Chang, J., Li, R., Jin, Y., Ong, C., Zhuo, S., Wang, P., 2019. Simultaneous production of fresh water and electricity via multistage solar photovoltaic membrane distillation. Nature Communications 10, 3012.
- Wang, X., He, Y., Liu, X., Cheng, G., Zhu, J., 2017c. Solar steam generation through bio-inspired interface heating of broadband-absorbing plasmonic membranes. Applied Energy 195, 414–425.
- Wang, X., Hsieh, M.L., Bur, J.A., Lin, S.Y., Narayanan, S., 2020. Capillary-driven solar-thermal water desalination using a porous selective absorber. Materials Today Energy 17, 100453
- Wang, Y., Wang, C., Song, X., Huang, M., Megarajan, S.K., Shaukat, S.F., Jiang, H., 2018a. Improved light-harvesting and thermal management for efficient solar-driven water evaporation using 3D photothermal cones. Journal of Materials Chemistry A 6, 9874–9881.
- Wang, Y., Wang, C., Song, X., Megarajan, S.K., Jiang, H., 2018b. A facile nanocomposite strategy to fabricate a rGO–MWCNT photothermal layer for efficient water evaporation. Journal of Materials Chemistry A 6, 963–971.
- Wang, Y., Zhang, L., Wang, P., 2016. Self-Floating Carbon Nanotube Membrane on Macroporous Silica Substrate for Highly Efficient Solar-Driven Interfacial Water Evaporation. ACS Sustainable Chemistry & Engineering 4, 1223–1230.
- Wang, Z., Yu, K., Gong, S., Mao, H., Huang, R., Zhu, Z., 2021. Cu3BiS3/MXenes with Excellent Solar–Thermal Conversion for Continuous and Efficient Seawater Desalination. ACS Applied Materials & Interfaces 13, 16246–16258.
- Wang, Z.L., Chen, J., Lin, L., 2015. Progress in triboelectric nanogenerators as a new energy technology and self-powered sensors. Energy & Environmental Science 8, 2250–2282
- Webb, J.A., Bardhan, R., 2014. Emerging advances in nanomedicine with engineered gold nanostructures. Nanoscale 6, 2502–2530.
- Wu, J., Zodrow, K.R., Szemraj, P.B., Li, Q., 2017a. Photothermal nanocomposite membranes for direct solar membrane distillation. Journal of Materials Chemistry A 5, 23712–23719.
- Wu, X., Chen, G.Y., Zhang, W., Liu, X., Xu, H., 2017b. A Plant-Transpiration-Process-Inspired Strategy for Highly Efficient Solar Evaporation. Advanced Sustainable Systems 1, 1700046.
- Xi, J.Q., Schubert, M.F., Kim, J.K., Schubert, E.F., Chen, M., Lin, S.-Y., Liu, W., Smart, J.A., 2007. Optical thin-film materials with low refractive index for broadband elimination of Fresnel reflection. Nature Photonics 1, 176.
- Xia, Y., Halas, N.J., 2011. Shape-Controlled Synthesis and Surface Plasmonic Properties of Metallic Nanostructures. MRS Bulletin 30, 338–348.
- Xiong, F., Zhang, J., Zhu, Z., Yuan, X., Qin, S., 2015. Ultrabroadband, More than One Order Absorption Enhancement in Graphene with Plasmonic Light Trapping. Scientific Reports 5, 16998.

- Xu, N., Hu, X., Xu, W., Li, X., Zhou, L., Zhu, S., Zhu, J., 2017a. Mushrooms as Efficient Solar Steam-Generation Devices. Advanced Materials 29, 1606762.
- Xu, N., Hu, X., Xu, W., Li, X., Zhou, L., Zhu, S., Zhu, J., 2017b. Mushrooms as Efficient Solar Steam-Generation Devices. Adv Mater 29.
- Xu, Y., Wang, J., Yu, F., Guo, Z., Cheng, H., Yin, J., Yan, L., Wang, X., 2020. Flexible and Efficient Solar Thermal Generators Based on Polypyrrole Coated Natural Latex Foam for Multimedia Purification. ACS Sustainable Chemistry & Engineering 8, 12053–12062.
- Xue, G., Liu, K., Chen, Q., Yang, P., Li, J., Ding, T., Duan, J., Qi, B., Zhou, J., 2017a. Robust and Low-Cost Flame-Treated Wood for High-Performance Solar Steam Generation. ACS Applied Materials & Interfaces 9, 15052–15057.
- Xue, G., Liu, K., Chen, Q., Yang, P., Li, J., Ding, T., Duan, J., Qi, B., Zhou, J., 2017b. Robust and Low-Cost Flame-Treated Wood for High-Performance Solar Steam Generation. ACS Appl Mater Interfaces 9, 15052–15057.
- Xue, G., Xu, Y., Ding, T., Li, J., Yin, J., Fei, W., Cao, Y., Yu, J., Yuan, L., Gong, L., Chen, J., Deng, S., Zhou, J., Guo, W., 2017c. Water-evaporation-induced electricity with nanostructured carbon materials. Nat Nanotechnol 12, 317–321.
- Xue, G., Xu, Y., Ding, T., Li, J., Yin, J., Fei, W., Cao, Y., Yu, J., Yuan, L., Gong, L., Chen, J., Deng, S., Zhou, J., Guo, W., 2017d. WATER-EVAPORATION-INDUCED ELECTRICITY WITH NANOSTRUCTURED CARBON MATERIALS. NATURE NANOTECHNOLOGY 12, 317–321
- Yang, P., Liu, K., Chen, Q., Li, J., Duan, J., XUE, G., XU, Z., XIE, W., ZHOU, J., 2017. SOLAR-DRIVEN SIMULTANEOUS STEAM Production AND ELECTRICITY GENERATION FROM SALINITY. ENERGY & ENVIRONMENTAL SCIENCE 10, 1923–1927.
- Yang, Y., Zhao, R., Zhang, T., Zhao, K., Xiao, P., Ma, Y., Ajayan, P.M., Shi, G., Chen, Y., 2018. GRAPHENE-BASED STANDALONE SOLAR ENERGY CONVERTER FOR WATER DESALINATION AND PURIFICATION. ACS NANO 12, 829–835.
- Ye, M., Jia, J., Wu, Z., Qian, C., Chen, R., O'brien, P.G., Sun, W., Dong, Y., Ozin, G.A., 2017. SYnthesis of Black TiOxNanoparticles by Mg Reduction of TiO2Nanocrystals and their Application for Solar Water Evaporation. Advanced Energy Materials 7, 1601811.
- Yin, H., Xie, H., Liu, J., Zou, X., Liu, J., 2021. Graphene tube shaped photothermal layer for efficient solar-driven interfacial evaporation. Desalination 511, 115116.
- Yu, F., Chen, Y., Liang, X., Xu, J., Lee, C., Liang, Q., Tao, P., Deng, T., 2017. Dispersion stability of thermal nanofluids. Progress in Natural Science: Materials International 27, 531–542.
- Yu, H., Peng, Y., Yang, Y., Li, Z.-Y., 2019. Plasmon-enhanced light–matter interactions and applications. npj Computational Materials 5, 45.
- Yu, S., Zhang, Y., Duan, H., Liu, Y., Quan, X., Tao, P., Shang, W., Wu, J., Song, C., Deng, T., 2015. The impact of surface chemistry on the performance of localized solar-driven evaporation system. Sci Rep 5, 13600.
- Zhang, B., Jie, J., Zhang, X., Ou, X., Zhang, X., 2017a. Large-Scale Fabrication of Silicon Nanowires for Solar Energy Applications. ACS Applied Materials & Interfaces 9, 34527–34543
- Zhang, C., Yan, C., Xue, Z., Yu, W., Xie, Y., Wang, T., 2016a. Shape-Controlled Synthesis of High-Quality Cu7S4 Nanocrystals for Efficient Light-Induced Water Evaporation. Small 12, 5320–5328.
- Zhang, J.-B., Ding, L., Wang, Y.-P., Zhang, L., Wu, J.-L., Zheng, H.-Y., Fang, L., 2016b. Theoretical studies on particle shape classification based on simultaneous small forward angle light scattering and aerodynamic sizing. Chinese Physics B 25, 034201.
- Zhang, P., Li, J., Lv, L., Zhao, Y., Qu, L., 2017b. Vertically Aligned Graphene Sheets Membrane for Highly Efficient Solar Thermal Generation of Clean Water. ACS Nano 11, 5087–5093.
- Zhang, P., Liao, Q., Yao, H., Cheng, H., Huang, Y., Yang, C., Jiang, L., Qu, L., 2018a. Three-dimensional water evaporation on a macroporous vertically aligned graphene pillar array under one sun. Journal of Materials Chemistry A 6, 15303–15309.

- Zhang, P., Liao, Q., Zhang, T., Cheng, H., Huang, Y., Yang, C., Li, C., Jiang, L., Qu, L., 2018b. High throughput of clean water excluding ions, organic media, and bacteria from defect-abundant graphene aerogel under sunlight. Nano Energy 46, 415–422
- Zhang, X., Zhang, T., An, X., Li, M., Pei, D., Zhang, J., Li, C., 2022. Guiding cellular channels of artificial nanohybrid woods for anisotropic properties and solar-thermal evaporation. Chemical Engineering Journal 428, 132060.
- Zhang, Y., Zhao, D., Yu, F., Yang, C., Lou, J., Liu, Y., Chen, Y., Wang, Z., Tao, P., Shang, W., Wu, J., Song, C., Deng, T., 2017c. Floating rGO-based black membranes for solar driven sterilization. Nanoscale 9, 19384–19389.
- Zhao, F., Guo, Y., Zhou, X., Shi, W., Yu, G., 2020a. Materials for solar-powered water evaporation. Nature Reviews Materials 5, 388–401.
- Zhao, H.-Y., Zhou, J., Yu, Z.-L., Chen, L.-F., Zhan, H.-J., Zhu, H.-W., Huang, J., Shi, L.-A., Yu, S.-H., 2020b. Lotus-Inspired Evaporator with Janus Wettability and Bimodal Pores for Solar Steam Generation. Cell Reports Physical Science 1, 100074.
- Zhao, X., Chen, Y., Yin, Y., Zou, L., Chen, Q., Liu, K., Lin, P., Su, H., Chen, Y., 2021. Janus Polypyrrole Nanobelt@Polyvinyl Alcohol Hydrogel Evaporator for Robust Solar-Thermal Seawater Desalination and Sewage Purification. ACS Applied Materials & Interfaces 13, 46717–46726.
- Zhou, L., Li, X., Ni, G.W., Zhu, S., Zhu, J., 2019. The revival of thermal utilization from the Sun: interfacial solar vapor generation. National Science Review 6, 562–578.
- Zhou, L., Tan, Y., Ji, D., Zhu, B., Zhang, P., Xu, J., Gan, Q., Yu, Z., Zhu, J., 2016a. Self-assembly of highly EFFICIENT, broadband plasmonic absorbers for solar steam generation. Science Advances 2, e1501227.
- Zhou, L., Tan, Y., Wang, J., Xu, W., Yuan, Y., Cai, W., Zhu, S., Zhu, J., 2016b. 3D self-assembly of aluminium nanoparticles for plasmon-enhanced solar desalination. Nature Photonics 10, 393–398.
- Zhu, G., Xu, J., Zhao, W., Huang, F., 2016. Constructing Black Titania with Unique Nanocage Structure for Solar Desalination. ACS Appl Mater Interfaces 8, 31716–31721.
- Zhu, L., Ding, T., Gao, M., Peh, C.K.N., Ho, G.W., 2019. Shape Conformal and Thermal Insulative Organic Solar Absorber Sponge for Photothermal Water Evaporation and Thermoelectric Power Generation. Advanced Energy Materials 9, 1900250.
- Zhu, L., Gao, M., Peh, C., Ho, G., 2018a. Solar-driven photothermal nanostructured materials designs and prerequisites for evaporation and catalysis applications. Materials Horizons 5.
- Zhu, L., gao, M., Peh, C., Wang, X.-Q., HO, G., 2018b. Self-Contained Monolithic Carbon Sponges for Solar-Driven Interfacial Water Evaporation Distillation and Electricity Generation. Advanced Energy Materials 8, 1702149.
- Zhu, L., Gao, M., Peh, C.K.N., Ho, G.W., 2018c. Solar-driven photothermal nanostructured materials designs and prerequisites for evaporation and catalysis applications. Materials Horizons 5, 323–343.
- Zhu, L., Gao, M., Peh, C.K.N., Wang, X., Ho, G.W., 2018d. Self-Contained Monolithic Carbon Sponges for Solar-Driven Interfacial Water Evaporation Distillation and Electricity Generation. Advanced Energy Materials 8, 1702149.
- Zhu, M., Li, Y., Chen, F., Zhu, X., Dai, J., Li, Y., Yang, Z., Yan, X., Song, J., Wang, Y., Hitz, E., Luo, W., Lu, M., Yang, B., Hu, L., 2018e. Plasmonic Wood for High-Efficiency Solar Steam Generation. Advanced Energy Materials 8, 1701028.
- Zhu, M., Li, Y., Chen, G., Jiang, F., Yang, Z., Luo, X., Wang, Y., Lacey, S.D., Dai, J., Wang, C., Jia, C., Wan, J., Yao, Y., Gong, A., Yang, B., Yu, Z., Das, S., Hu, L., 2017. Tree-Inspired Design for High-Efficiency Water Extraction. Advanced Materials 29, 1704107.
- Zielinski, M.S., Choi, J.W., La Grange, T., Modestino, M., Hashemi, S.M., Pu, Y., Birkhold, S., Hubbell, J.A., Psaltis, D., 2016. Hollow Mesoporous Plasmonic Nanoshells for Enhanced Solar Vapor Generation. Nano Lett 16, 2159–2167.